Paleonutrient and productivity records from the subarctic North Pacific for Pleistocene glacial terminations I to V

Holger Gebhardt,[1,2] Michael Sarnthein,[1] Pieter M. Grootes,[3] Thorsten Kiefer,[1,4,5] Hartmut Kuehn,[1] Frank Schmieder,[6] and Ursula Röhl[6]

Received 29 June 2007; revised 1 July 2008; accepted 14 July 2008; published 22 November 2008.

[1] Our study addresses fundamental questions of the mode and timing of orbital and millennial-scale changes in the meridional overturning circulation (MOC) of the subarctic North Pacific. Particular concerns are the vertical mixing, the present and past abundance of nutrients in surface waters despite strong stratification, and the North Pacific–North Atlantic seesaw of oscillations in sea surface temperature (SST). We do this by generating and interpreting multiple records for glacial terminations I–V down two long piston cores, one each from the western and eastern subarctic Pacific. Chlorins and biogenic opal are proxies for surface water productivity; $\delta^{13}C$ of epibenthic foraminifera is a record of deepwater ventilation; and the $\delta^{13}C$ of *N. pachyderma* sin. is a tracer of nutrients in subsurface waters that extend up to the sea surface during times of vertical mixing. The degree of mixing is traced by pairing SST and $\delta^{18}O$ records of planktic surface and subsurface (pycnocline) dwellers. Tight age control is deduced from a suite of age-calibrated ^{14}C plateau boundaries for Termination I and benthic $\delta^{18}O$ and geomagnetic events for the last 800 ka. Carbon 14 paleoreservoir ages record the ages of surface and deep waters to uncover short-term changes in MOC over Termination I. We have defined a standard sequence of short-term productivity events for Termination I, also evident during terminations II to V and subsequent interglacials over the last 450 ka. The peak glacial regime of stable stratification and low productivity terminated, together with the end of ice rafting and melting, near 17 ka, ~2000 years after the onset of Termination I. Pulses of vertical mixing and incursion of warm surface waters from the subtropics followed. Convected young water masses finally penetrated down to 3600-m water depth at 17.0 to less than 14.5 ka, significantly improving bottom water ventilation through the late deglacial and earliest interglacial. Mixing with upwelled nutrients from the pycnocline induced short-term maxima in algal production of chlorins and biogenic opal near 17–15 and 15–12 ka, respectively. Deglacial meltwater incursions in the Aleutian Current and silica input from North American rivers also promoted East Pacific productivity after 15.5 ka. Productivity decreased during the late deglacial and early interglacial, coeval with an exceptional peak in $CaCO_3$ preservation caused by both low organic flux and well-ventilated deepwater. Subsequently, low salinity and cool surface waters and in turn, stratification were gradually restored. A second, opal-dominated productivity maximum marked the ends of interglacials. The deglacial pulses of vertical mixing around 17–11 ka imply an important contribution of the North Pacific to the coeval release of oceanic CO_2 into the atmosphere and support the east-west seesaw model of climate change.

Citation: Gebhardt, H., M. Sarnthein, P. M. Grootes, T. Kiefer, H. Kuehn, F. Schmieder, and U. Röhl (2008), Paleonutrient and productivity records from the subarctic North Pacific for Pleistocene glacial terminations I to V, *Paleoceanography*, *23*, PA4212, doi:10.1029/2007PA001513.

1. Introduction

[2] Today, a steep halocline in the subarctic North Pacific Ocean impedes mixing of surface waters with underlying nutrient-rich Pacific Deepwater [*Warren*, 1983; *Clarke et al.*, 2001]. Low surface water salinity results from excess precipitation over evaporation over both the ocean and adjacent continents that produce continental runoff, which especially applies to British Columbia as recorded by the salinity pattern of the Aleutian Current [*Warren*, 1983]. Further freshwater comes from the melt of winter sea ice and continental ice sheets.

[3] In spite of the low-salinity surface layer that impedes intense nutrient supply from below, the modern subarctic North Pacific forms a major source of oceanic CO_2, with net fluxes reaching up to 4 moles CO_2 m^{-2} a^{-1} [*Takahashi et al.*, 2002]. Deep convection during periods of intensified primary productivity may have strongly increased advection of CO_2-rich water from the deep and have resulted in enhanced CO_2 release to the atmosphere on a regional scale

[1]Institut für Geowissenschaften, University of Kiel, Kiel, Germany.
[2]Now at Geologische Bundesanstalt, Wien, Austria.
[3]Leibniz Laboratory, University of Kiel, Kiel, Germany.
[4]Department of Earth Sciences, University of Cambridge, Cambridge, UK.
[5]Now at PAGES International Project Office, Bern, Switzerland.
[6]Center for Marine Environmental Sciences, University of Bremen, Bremen, Germany.

0883-8305/08/2007PA001513

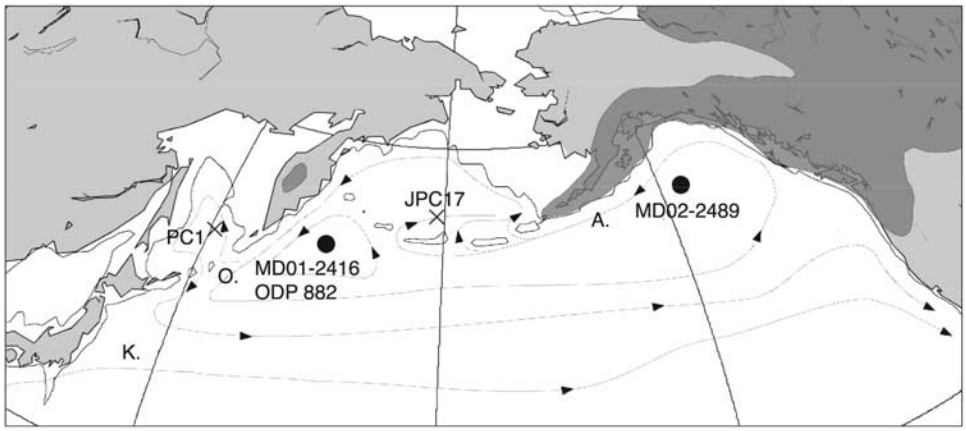

Figure 1. Locations of ODP Site 882 and Marion Dufresne (MD) sites MD01-2416 and MD02-2489 on Emperor and Patton Seamounts and of cores JPC17 in the Bering Sea [*Brunelle et al.*, 2007] and PC1 in the Sea of Okhotsk [*Sato et al.*, 2002]. Bold contour line delineates 100-m water depth, and dark areas outline glacial ice sheets. Dotted lines with arrows mark surface water currents [*Dodimead et al.*, 1963], and capital letters indicate the northern Oyashio (O.) and southern Kuroshio (K.) currents in the western North Pacific and the Aleutian Current (A.) in the northeast.

across the entire subarctic Pacific covering >80° longitude. The dynamical and biogeochemical history of this region may thus be of great significance for paleoceanographic modeling and climate reconstructions, in particular for understanding the mechanisms of rapid oceanic CO_2 release [*Sigman and Boyle*, 2000].

[4] On the basis of a major long-term reduction in the accumulation of opal and an increase in the $\delta^{15}N$ of organic matter 2.73 Ma, *Haug et al.* [1999] and *Sigman et al.* [2004] inferred that stable Quaternary stratification of the subarctic North Pacific started as a self-sustained, quasi-permanent feature with the onset of major Northern Hemisphere glaciation. Recently, the stratification was restricted to Quaternary glacial and late interglacial periods only [*Jaccard et al.*, 2005; *Sarnthein et al.*, 2005, 2006].

[5] Orbital-scale changes in stratification may be linked in the subarctic North Pacific to its location near the terminus of global ocean thermohaline circulation (THC) [*Broecker*, 1991]. Increased overturning rates in Atlantic source regions of THC (Greenland Sea) may have enhanced the deepwater incursion into the Pacific from the Southern Ocean, extending up to the subarctics [*Schlosser et al.*, 2001] and entailing regional-scale upwelling along the northern margins, as was assumed [*Gordon*, 1991; *Schmitz*, 1995] and established for the present day by *Southon et al.* [2005]. Vertical admixture of old, nutrient-rich Pacific Deepwater to the nutrient-depleted surface waters would result in increased plankton productivity.

[6] However, massive nutrient supply may also result from a warming of subarctic surface waters and/or reduced freshwater advection, leading to a lowered precipitation/evaporation balance that in turn promotes vertical mixing across a weakened North Pacific pycnocline, as suggested by *Sarmiento et al.* [2004]. In contrast to the first model this process will lead to reversed THC in the far northwestern Pacific Ocean, a scenario recently confirmed by extremely low planktic and benthic ^{14}C reservoir ages in the subarctic North Pacific for most of Termination Ia and later on [*Sarnthein et al.*, 2007, 2004]. Modern stable stratification in the subarctic Pacific Ocean may thus have been replaced by vertical mixing and intensified downwelling over distinct time intervals 17.5–11.0 ka, coeval with Heinrich 1 (H1), Bølling-Allerød (B/A), and Younger Dryas (YD) to earliest Holocene times.

[7] High plankton productivity leads to increased accumulation of algal products (e.g., chlorin pigments and diatom frustules) in deep North Pacific sediments. Records of these productivity tracers may therefore help unravel the complex causes for changes in North Pacific primary productivity. High nutrients in surface and/or subsurface waters, in turn, are reflected by lowered $\delta^{13}C$ values in shell calcite of subpolar planktic foraminifera; these values depend on their dominant habitats [*Simstich et al.*, 2002]. High $\delta^{15}N$ values of organic matter may record increased surface water nutrient utilization [*Galbraith et al.*, 2008; *Brunelle et al.*, 2007]. Sediment records of variations in surface water temperature (SST), transport of ice-rafted debris (IRD), and the epibenthic $\delta^{13}C$ record of bottom water ventilation provide complementary evidence of contemporary paleoceanographic regimes.

[8] *Haug et al.* [1999], *Jaccard et al.* [2005], and *Brunelle et al.* [2007] used variations in biogenic opal, biogenic Ba, and/or $\delta^{15}N$ to generate the first high-resolution paleoproductivity records that cover several Pleistocene glacial cycles in the open subarctic North Pacific (ODP Site 882) and Bering Sea (JPC17; Figure 1). An array of benthic $\delta^{13}C$ records of deep and intermediate water ventilation and opal and organic-carbon-based paleoproductivity records were published for the last 25 ka, in particular for glacial Termination I [*Keigwin et al.*, 1992; *Keigwin*, 1998; *Zahn et al.*, 1991; *Sarnthein et al.*, 2006], where they document a paramount productivity spike. Further records were established for the Okhotsk adjacent sea (e.g., PC1, Figure 1)

[*Sato et al.*, 2002]. However, the findings of these studies won't necessarily apply to the open subarctic North Pacific.

[9] Our study aims to identify the diverse mechanisms of nutrient supply, which led to major increases of surface water productivity in the western and eastern subarctic Pacific over deglacial and interglacial times. We reconstruct specific successions of paleoceanographic changes for each of the last five glacial terminations, and deduce important evidence for a better understanding of the suite of oceanographic and climatic changes that governed deglacial and peak interglacial times. The changes include vertical mixing, full reversals in meridional overturning, and short-term strong increases in nutrient inventories in a major high-latitude region of the global ocean [*Sigman et al.*, 2004; *Sarnthein et al.*, 2001, 2007].

2. Materials, Methods, and Rationales for Sediment Proxies

[10] Because of controversies about the value of the proxies crucial to understand paleonutrients and paleoproductivity, we have included some discussion to justify the techniques that we prefer and of those about which we have doubts.

2.1. Core Material

[11] Our records use sediments retrieved in two giant piston cores retrieved from the subpolar North Pacific Ocean (Figure 1). N.S. Marion Dufresne IMAGES Core MD01-2416 from Detroit Seamount (51.268°N, 167.725°E, 2317 m; near to ODP Site 882) is 44.75 m long, and Core MD02-2489 from Patton Seamount (54.390°N, 148.921°W, 3640-m water depth) is 29.8 m long. Core depths are given in cm below sea floor (cm bsf). Lithologic descriptions of the sediments (various mixtures of siliciclastic mud and siliceous and calcareous ooze) are shown in Figures S1 and S2.[1]

[12] Piston cores stretch the sediment near the top by up to >30% [*Széréméta et al.*, 2004]. Thus, sedimentation rates calculated for the upper few meters may be too high. For both our cores, this issue applies to the Holocene and glacial Termination I, where we have the most complete and highest resolving data sets down to 250 cm bsf.

2.2. Stable Oxygen and Carbon Isotopes

[13] We picked planktic and benthic foraminifera from sieved samples of sediment and analyzed them for oxygen and carbon isotopes. Planktic records were generated using the surface dweller *Globigerina bulloides* (in both cores down to 250 cm bsf only) and *Neogloboquadrina pachyderma* sin., a subsurface dweller close to the pycnocline. The benthic record in Core MD01-2416 was generated using *Uvigerina* spp. (mainly *U. senticosta* and *U. hispida*), since this genus occurs continuously throughout the core (data from *Sarnthein et al.* [2004, 2005], supplemented). However, *Uvigerina* is too scarce for generating a continuous record in Core MD02-2489. For Termination I, we examined the epibenthic genus *Cibicidoides* spp. (mostly *C. kullenbergi*). In both cores this genus only occurs abundantly in the top sections.

[14] For actual analyses, we picked multiple specimens from each sample. These aliquots comprised about 30 specimens of *N. pachyderma* sin. from the 150-to-250-μm fraction, 20 to 30 specimens of *G. bulloides* from the >150 μm fraction, 5 to 10 specimens of *Uvigerina* spp. (various monospecific samples) and 1 to 16 specimens of *Cibicidoides* spp. each from the >250-μm fraction. Foraminifera tests were treated with 98.8% ethanol, cracked, and ultrasonically cleaned following standard procedures. Stable carbon and oxygen isotopes were measured on a Finnigan MAT 251 mass spectrometer at the Leibniz-Labor (Kiel), coupled online to the Carbo-Kiel device I for automated CO_2 preparation. External precision is better than 0.07‰ and 0.04‰ for oxygen and carbon, respectively. Data are given in conventional delta notation versus PeeDee Belemnite (PDB) standard.

2.3. Benthic δ^{18}O Brinewater Signals

[15] The (epi-) benthic δ^{18}O record of MD01-2416 (60–110 cm bsf) contains a number of short-term (seasonal to decadal), very negative outliers of 0.5–1.0‰, that are based on 1 to 6 specimens of *Cibicidoides* spp. each and can be explained neither by short-term increased temperature nor by decreased salinity of bottom water. Likewise, a series of ^{14}C ages [*Sarnthein et al.*, 2007], radiography, and proxy data suggest that downcore bioturbation of foraminiferal specimens with a Holocene δ^{18}O signature down to these core depths is rather unlikely. By analogy with δ^{18}O records from the Nordic Seas [*Bauch and Bauch*, 2001] we interpret the abrupt benthic δ^{18}O shifts of −1.0 to −1.5‰ as the result of brinewater pulses that have been induced by seasonal sea ice formation in meltwater-influenced surface waters with reduced salinity such as in the modern Sea of Okhotsk, a process that does not imply isotopic fractionation.

2.4. Tracers of Nutrient Concentration and Bottom Water Ventilation

[16] Stable carbon isotope ratios (δ^{13}C) of the epibenthic foraminiferal genera *Cibicidoides* and *Planulina* have been established as tracers of PO_4 nutrient concentrations and ventilation of ocean water [*Lynch-Stieglitz*, 2003]. A similar interpretation may apply to a large set of published and unpublished planktic data from sediment traps and core tops in ocean regions as different as the northern and equatorial Atlantic [e.g., *Simstich*, 1998; *Deuser et al.*, 1981a, 1981b; *Ganssen*, 1983], the Arabian Sea, and South China Sea [*Wang et al.*, 1999]. Overall, the spatial distribution patterns of these data suggest that δ^{13}C values of various planktic foraminifera species primarily reflect the nutrient concentrations in ocean surface water ambient to shell calcification, besides various secondary forcings such as air-sea exchange of CO_2, sea surface temperature, secular δ^{13}C variations, and vital and metabolic effects.

[17] This conclusion is based on the following evidence:

[18] 1. Low δ^{13}C of *N. pachyderma* sin. clearly delineates nutrient maxima near the pycnocline in stratified surface waters of the modern and late Pleistocene northern North Atlantic [*Sarnthein et al.*, 1995; *Simstich et al.*, 2002].

[1] Auxiliary materials are available in the HTML. doi:10.1029/2007PA001513.

[19] 2. Differing from theory [*Lynch-Stieglitz*, 2003], extreme changes in air-sea exchange of CO_2 only lead to minor variations in $\delta^{13}C$ values of *N. pachyderma* sin. They amount to 0.3–0.6‰ in subsurface waters of the highly stratified late Holocene subarctic Pacific, today a source of atmospheric CO_2 [*Takahashi et al.*, 2002], but only differ by 0.3‰ from 0.5–0.9‰ $\delta^{13}C$ found in *N. pachyderma* sin. of modern Arctic Water in the Nordic Seas. This site of major deepwater convection forms a sink of atmospheric CO_2, thus implying far more ^{13}C-enriched values.

[20] 3. A secular effect of 0.3‰ for interglacial-to-glacial changes in preformed nutrients [*Duplessy et al.*, 1988] was not reproducible in later reconstructions of Atlantic epibenthic $\delta^{13}C$ variations from glacial-to-interglacial times [*Sarnthein et al.*, 1994].

[21] 4. The metabolic and vital effects of $\delta^{13}C$ values of *N. pachyderma* sin. are well constrained by a shift of ~0.83‰ versus $\delta^{13}C$ in dissolved inorganic carbon (DIC) [*Labeyrie and Duplessy*, 1985].

[22] 5. However, problems arise from the different habitats of planktic foraminifera, since *N. pachyderma* sin. is dwelling deep, close to the pycnocline in stratified sea regions. Thus the $\delta^{13}C$-based paleonutrient record of *N. pachyderma* sin. cannot be compared directly with surface water records of paleoproductivity, except for times of strong vertical mixing. Also, $\delta^{13}C$ records of *N. pachyderma* sin. cannot be replaced by isotope records of the subpolar near-surface dweller *G. bulloides*, since the $\delta^{13}C$ signal of this species appears strongly controlled by various metabolic factors not adequately understood.

[23] As with $\delta^{13}C$, $\delta^{15}N_{bulk}$-based records (of bulk sediment) of nutrient utilization in surface waters (which we have not measured) also form a complex proxy. *Galbraith et al.* [2008] show a raw $\delta^{15}N_{bulk}$ record which suggests that relative nutrient utilization at Site MD01-2416 was almost complete during early, peak, and deglacial times, and decreased only a little during early H1 and the last 10 ka (poorly age-constrained), in contrast to very little nutrient utilization over interglacial MIS 5.5–4.2. To take care of the apparent problem, background signals linked to changes in the denitrification of the equatorial Pacific were removed from this record to reveal the actual variations in the unutilized surface nitrate pool of the open subarctic Pacific, today the heart of a high-nutrient, low-carbon region. For this reason, the $\delta^{15}N$ proxy of relative nutrient utilization was refined by subtracting a ''general North Pacific'' $\delta^{15}N_{nitrate}$ component from the subarctic western Pacific $\delta^{15}N_{bulk}$ record. However, this novel approach requires heroic chronostratigraphic assumptions that we have problems to follow. The slightest shifts in the highly controversial age control near glacial terminations, that are intervals of major and rapid ocean change, may already produce entirely different $\delta^{15}N$ anomalies.

2.5. Total Organic Carbon and Chlorin Concentration as Paleoproductivity Proxies

[24] Since work by *Müller and Suess* [1979] various authors have demonstrated that accumulation rates of marine total organic carbon (TOC) and chlorins (pigments from chlorophyll used as a tracer of marine TOC) form reliable records of algal productivity and TOC flux rates in deep sea sediments [*De La Rocha*, 2007], although in part also controlled by differential rates of siliciclastic sediment input. In contrast, no correlation is seen between TOC burial efficiency and oxygenation. We believe that the small changes in bottom water ventilation in the open ocean and the impact of low oxygenation are insufficient to control open ocean TOC accumulation rates [*Calvert et al.*, 1987; *Sarnthein et al.*, 1992; *Hedges and Keil*, 1995]. Moreover, TOC on the seafloor is subject to a suite of different, in part bacterial, oxidation processes acting at different states of bottom water ventilation, even at low oxygenation levels [*De La Rocha*, 2007]. Finally, short-term maxima in chlorin/TOC preservation in the subarctic North Pacific do not parallel any $\delta^{13}C$ and ^{14}C-based minima in bottom water ventilation, and vice versa; rather the opposite is found. Also, high and low contents of chlorin and TOC match many corresponding changes in the accumulation rate of biogenic opal, a further productivity tracer, the preservation of which is independent of bottom water oxygenation. Thus chlorin content is employed as a prime record of past plankton productivity.

[25] TOC contents in MD01-2416 were measured by gas chromatography with a CHN-O elemental analyzer (Carlo Erba Instruments) on 10 mg sediment, TOC in MD02-2489 by coulometric titration. Inorganic carbon was removed with H_3PO_4 for TOC analyses; values are reproduced within ±0.2 weight % (wt%). Chlorin contents closely parallel TOC values in sediment samples from Termination I (Figure 3), suggesting that marine algae are the dominant contributor to TOC.

[26] Chlorin contents were calculated from CPE (chloroplastic pigment equivalents) values measured with a Turner-Fluorometer TD-700, applying the standard procedures of IFM-GEOMAR, Kiel. Pigments were released with acetone and a cell-mill from 100 mg of freeze-dried and crushed sediment, and acidified with HCl to change chlorophyll-*a* into phaeopigments. A Sigma-Aldrich 25730-chlorophyll-*a* solution was used to produce a standard for CPE measurements. Chlorin contents are given in ng g^{-1}.

2.6. Biogenic Opal as Paleoproductivity Proxy

[27] As shown by several authors [*Keigwin*, 1998; *Keigwin et al.*, 1992; *Crusius et al.*, 2004; *De La Rocha*, 2007], sediment accumulation rates of biogenic opal in the subarctic Pacific and elsewhere track past productivity. However, paleoproductivity records of biogenic opal don't need to match chlorin- and TOC-based records, since the relationship between PO_4 and SiO_2 as nutrients is close to exponential, showing a prominent, almost abrupt increase in silica at higher PO_4 concentrations [*Yool and Tyrrell*, 2003]. This increase is possibly linked to different dissolution and nutrient sources. Moreover, changing bottom water ventilation won't affect the preservation of biogenic opal in deep-sea sediments. However, excessive opal accumulation rates may derive from seasonally short-term enhanced flux rates of biogenic opal, that lead to enhanced opal preservation and a positive feedback.

[28] Contents of biogenic opal were measured at IFM-GEOMAR in Kiel following the automated leaching method

of *Müller and Schneider* [1993]. The opaline material was extracted from 2-mg samples of freeze-dried and crushed sediment by sodium hydroxide at ~85°C for ~45 min. The resulting extract was analyzed for dissolved silicon by molybdate-blue spectrophotometry, finally applying the mineral correction of *DeMaster* [1981]. Replicate measurements of opal resulted in an uncertainty of ±0.5 wt%.

[29] Weight % biogenic opal were recalculated into mass accumulation rates of opal, for glacial terminations I–V, to overcome effects of percentage dilution of radiolarian and diatom frustules by other sediment particles, which may obscure any productivity estimates [see also *Keigwin et al.*, 1992]. However, chronological uncertainties for terminations II–V may likewise impede the generation of robust estimates of accumulation rates. Thus our opal-based paleoproductivity estimates need to rely on both major percentage changes and rough estimates of accumulation rates, also presented for comparison with records elsewhere.

[30] Biogenic Ba (Ba_{bio}) forms a further much cited, although still controversial sediment proxy of paleoproductivity [*De La Rocha*, 2007; *Plewa et al.*, 2006]. *Jaccard et al.* [2005] established an XRF-based Ba_{bio} record for neighbor ODP Site 882. In our paper, this record is compared with other paleoproductivity records of MD01-2416, using a series of well-defined Ca spikes in both cores to correlate the different age models.

2.7. Ca XRF Intensity and $CaCO_3$ Contents

[31] $CaCO_3$ contents serve as proxy of bottom water corrosivity and hence of alkalinity. Nondestructive analyses of major elements such as Ca were performed with the X-ray fluorescence (XRF) Core Scanner I at Bremen University [*Röhl and Abrams*, 2000]. Ca intensity is given in counts per second (cps). In Core MD01-2416, measurements were recorded at 1-cm intervals from the core top down to 1200 cm bsf, and at 2-cm intervals below. XRF data were measured every 2 cm in Core MD02-2489.

[32] To assess the relationship between XRF counts of Ca and actual $CaCO_3$ values, we also measured the wt% $CaCO_3$ in roughly 150 samples from Core MD01-2416 from Termination I with a Carlo-Erba analyzer (see TOC), and 15 samples from Core MD02-2489 with coulometric titration. Replicate analyses reveal analytical uncertainties of 0.5–4.0 wt%. Trends in the Ca records generally correlate with those of $CaCO_3$ (Figure 3). Thus, changes in Ca provide a good proxy for variations in wt% $CaCO_3$. The accuracy of XRF core scanner measurements also depends on physical properties, especially the surface quality (e.g., rough or smooth) and the water content of the sediment. The detection limit of Ca is near 800 ppm. Accordingly, sediments with biogenic opal contents >15 wt% produce XRF counts of Ca that are weighed down by high contents of water and Si [*Tjallingii et al.*, 2007], and are much lower than $CaCO_3$ contents measured by conventional chemical analyses.

2.8. Sea Surface Temperature and Sea Surface Salinity

[33] Summer SSTs were reconstructed both from Mg/Ca ratios of selected planktic foraminifera species and from census counts of planktic foraminifera using the SIMMAX transfer function [*Pflaumann et al.*, 2003].

[34] Mg/Ca ratios were measured on monospecific samples of *N. pachyderma* sin. and *G. bulloides,* which were cleaned after the method of *Barker et al.* [2003] and analyzed with a Varian Vista inductively coupled plasma-atomic emission spectrometer [*de Villiers et al.*, 2002]. Mg/Ca ratios were converted into paleotemperatures of late spring and late summer (G. Haug, personal communication, 2007) using the species-specific calibration of *Elderfield and Ganssen* [2000]. Replicate analyses resulted in a reproducibility of approximately ±0.8°C (details of uncertainty are given by *Sarnthein et al.* [2004]).

[35] Unfortunately, modern reference data for the planktonic foraminifera transfer function from the northern North Pacific are supported by an insufficient number of data points [*Chen et al.*, 2005]. Thus we employed the Atlantic database of GLAMAP 2000 [*Pflaumann et al.*, 2003] to calibrate the composition of North Pacific faunal assemblages to caloric summer SST (i.e., July to September average in Northern Hemisphere) at 10-m water depth by means of the SIMMAX transfer function. The resulting SST estimates have analytical uncertainties of ±0.8°C.

[36] The actual uncertainties are much higher because of problems in species identification. North Pacific and North Atlantic morphospecies of *N. pachyderma* sin. represent genetically different cryptospecies [*Darling et al.*, 2003; *Kucera and Darling*, 2002; *Darling et al.*, 2006]. The North Pacific variety is a subpolar cryptospecies and represents warmer temperatures than its polar counterpart in the North Atlantic [*Darling et al.*, 2006]. Thus, SIMMAX SST reconstructions based on a North Atlantic database might be slightly too low (2–4°C?). However, the SIMMAX-based SST estimates are generally equal to or even warmer than corresponding paleotemperature estimates derived from Mg/Ca ratios. We therefore assume that the difference between actual SST (defined for 10-m depth; SIMMAX SST) and temperatures near the halocline, where most of *N. pachyderma* sin. and its Mg/Ca ratio are formed, may exceed the possibly systematic errors from using an Atlantic database for the North Pacific. The SIMMAX transfer function apparently is strongly muting any short-term SST oscillations [*Sarnthein et al.*, 2004].

[37] Rough estimates of sea surface salinity (SSS) changes near the surface and near the pycnocline, the habitats of *G. bulloides* and *N. pachyderma* sin., were obtained from the respective planktic $\delta^{18}O$ values. They were corrected for changes in global ice volume [*Labeyrie et al.*, 1987] and normalized for SST changes, following the techniques proposed by *Duplessy et al.* [1991a] and assuming that 1‰ $\delta^{18}O$ is equal to 3.57°C and 2.75 psu in local SSS [*Keigwin*, 1998].

2.9. Ice-Rafted Debris

[38] Abundances of ice-rafted debris (% IRD) were deduced from a grain count of aliquots of at least 300 grains in the >150-μm fraction of each sample. IRD grains are pebbles, rock fragments, quartz, and other mineral grains.

2.10. AMS ^{14}C Ages

[39] AMS ^{14}C ages were determined for 44 samples from Core MD02-2489 at the Leibniz Laboratory, Kiel University

Table 1. Summary of Uncorrected and Reservoir-Corrected Planktic and Benthic ^{14}C Ages[a]

Laboratory Number	MD02-2489 Core Depth (cm bsf)	Original ^{14}C Ages (years BP)	Error 1 s (±years)	Reservoir Age (years)	Reservoir Effect-Corrected ^{14}C Age (years BP)	Calendar Age (years BP)	Comments (Derivation of Ages)
				Planktic Ages			
KIA 23971	4,50	13790	80	??			reworked
KIA 24584	9,50	13590	70	??			reworked
KIA 23972	59,00	7570	40	?600	6970	7800	intcal04
KIA 34750	66,50	8715	45	?600	8115	9020	intcal04
KIA 34751	76,50	9210	50	?600	8610	9550	intcal04
KIA 34752	86,50	10140	70	?600	9540	10770	intcal04
KIA 34753	96,00	11080	60	?600	10480	12570	intcal04
KIA 25503	110,00	11870	30	?600	11270	13170	intcal04
KIA 34754	119,00	12120	70	?600	11520	13350	intcal04
KIA 25504	130,00	12730	35	550	12180	14200	plateau 1
KIA 35318	140,00	12840	70	550	12290	14397	plateau 1
KIA 26539	150,75	12918	65	550	12370	14609	plateau 1
KIA 35319	156,00	13250	70	550	12700	14713	plateau 1
KIA 26540	160,00	11935	45	550	11385	14791	plateau 1
KIA 34755	163,00	12920	90	550	12370	14850	plateau 1
KIA 35320	165,50	12800	90	550	12250	14900	plateau 1
KIA 34756	171,50	13820	80	1000	12820	15300	plateau 2
KIA 35321	177,50	13990	80	1000	12990	15590	plateau 2
KIA 34757	181,50	13850	80	1000	12850	15783	plateau 2
KIA 35322	184,50	14030	80	1000	13030	15928	plateau 2
KIA 35323	189,50	14180	80	1000	13180	16170	plateau 2
KIA 23973	192,00	14500	70	1000	13500	16290	plateau 2
KIA 35324	195,50	14270	80	1000	13270	16460	plateau 2
KIA 34758	200,50	14430	90	1000	13430	16730	plateau 2
KIA 35325	204,50	15050	90	1200	13850	16930	
KIA 35326	209,50	15580	90	1350	14230	17136	plateau 3
KIA 34759	212,50	15500	95	1350	14150	17245	plateau 3
KIA 35327	217,50	15350	90	1350	14000	17430	plateau 3
KIA 34760	223,50	16060	80	1600	14460	17652	
KIA 35328	231,00	16750	110/100	1700	15050	17938	plateau 4
KIA 35329	237,00	16830	110/100	1700	15130	18100	plateau 3
KIA 26541	248,00	16867	65	1700	15170	18500	plateau 3
KIA 34761	254,50	17300	90	1700	15600	18880	intcal04
KIA 26550	268,00	18042	65	1700	16340	19480	intcal04
KIA 26542	520,00	30521	170	?	?	33500	estimated
KIA 26551	600,75	39472	390/−375	?	?	41000	estimated
KIA 26543	684,00	43481	600/−560	?	?	44000	estimated
				Benthic Ages			
KIA 36127	129,00	13640	80	1480	13090	14135	plateau 1
KIA 36128	164,00	14790	90	2420	14240	14880	plateau 1
KIA 36129	173,50	15620	100	2700	14620	15400	plateau 2
KIA 36710	196,00	15810	110	2540	15810	16500	plateau 2
KIA 36130	200,00	15080	100	1650	14080	16930	
KIA 36711	205,00	15450	100	1600	14250	16960	plateau 2/3
KIA 36131	217,50	17090	135	3090	15740	17430	plateau 3
KIA 36132	229,00	18120	120	3140	16420	17860	plateau 4
KIA 36133	250,00	18470	130	3270	16770	18570	plateau 4

[a]Calendar ages are deduced from age-calibrated plateau boundaries (details of age conversion are given by *Sarnthein et al.* [2007]) and from Intcal04 [*Reimer et al.*, 2004]. Age uncertainty near the ^{14}C plateaus is ~200 years, and ^{14}C reservoir ages are derived from plateau tuning for Core MD02-2489.

(Table 1). 37 samples used 3–8 mg carbonate each from planktic foraminifera; 9 ages were measured on benthic foraminifera. The large number and specific selection of samples enables proper identification of ^{14}C plateaus characteristic of the last deglacial, with an average dating resolution of ~200 years. Carbon 14 ages for Core MD01-2416 were provided from *Sarnthein et al.* [2007]. High-precision dating was enabled by careful cleaning and preparation of foraminifera samples, and by the use of separate planktic foraminifera samples from MIS 5.5 in Core MD01-2416 to measure the ^{14}C value of local "dead carbon" for background correction (through subtraction).

2.11. Paleomagnetism

[40] Paleomagnetism of MD01-2416 was analyzed both on discrete samples from selected core intervals, and continuously on 1.5-m-long core halves, where Natural Remanent Magnetization (NRM) was measured in U channels using a 2G Enterprises cryogenic magnetometer at the University of Bremen. With both approaches, characteristic Remanent Magnetization (ChRM) was deduced from stepwise alternating field demagnetization at 11 different applied fields up to 80 mT. Inclination of ChRM was derived through the algorithm of *Kirschvink* [1980]. Anhysteretic remanent magnetization (ARM) was imparted at a constant alternating

Table 2. Average Sampling Resolution of Paleoceanographic and Paleoproductivity Records for Terminations I to V in Cores MD01-2416 and MD02-2489[a]

	Terminations (MIS)					
Proxy	MD01-2416 I (1–2.2)	II (5.5–6.2)	III (7.5)	IV (9.3–10.2)	V (11.1–12)	MD02-2489 I (1–2)
δ^{13}C, δ^{18}O *N. pachyderma* s	0.06	0.46	0.29	0.89	1.03	0.13
δ^{18}O *G. bulloides*	0.31	-	-	-	-	0.13
Biogenic opal	0.13	0.92	1.23	1.16	1.74	0.61
Chlorin	0.20	1.00	0.58	1.69	2.44	0.31
Ca (XRF)	0.07	0.31	0.22	0.67	1.04	0.13
$CaCO_3$	0.07	-	-	-	-	0.59
SIMMAX SST	0.15	1.14	0.68	1.16	1.03	0.39
IRD	0.19	0.61	0.68	1.34	1.03	0.25
δ^{13}C, δ^{18}O *Cibicidoides* spp.	0.09	-	-	-	-	0.13
δ^{18}O *Uvigerina* spp.	0.06	0.39	0.42	0.75	0.66	-
Mg/Ca *N. pachyderma* s	0.12	-	-	-	-	0.49
Mg/Ca *G. bulloides*	-	-	-	-	-	0.48
TOC	0.07	-	-	-	-	0.61

[a]Average sampling resolution is given in 1000 years per sample. Arabian numerals in brackets refer to marine isotope stages (MIS). XRF is X-ray fluorescence. SIMMAX SST is sea surface temperature estimates for summer, based on planktic foraminifera census counts. IRD is ice-rafted debris. TOC is total organic carbon.

field of 100 mT with a bias field of 0.04 mT, and demagnetized in 9 steps up to 60 mT. The NRM/ARM record of relative geomagnetic paleointensity and ChRM inclination changes form the basis of our magnetostratigraphy.

2.12. Data Management

[41] All data sets are available from PANGAEA databank (http://www.pangaea.de/PangaVista).

3. Age Control

[42] Age control was based on three independent lines of evidence, on the basis of (1) ^{14}C plateau boundaries for Termination I, (2) high-resolution (Table 2), long-term benthic and planktic δ^{18}O records at sites MD01-2416 (*Sarnthein et al.* [2005], supplemented) and MD02-2489, and (3) a combination of geomagnetic paleointensity and inclination events in Core MD01-2416 (Table 3 and Figures 2 and S3).

[43] The ^{14}C record of MD01-2416 shows a suite of three distinct planktic ^{14}C plateaus (Figure S4a). As displayed by *Sarnthein et al.* [2007], six age-calibrated plateau boundaries enable us to identify six calendar age control points with uncertainties of 150–200 years for the early last deglacial, ~19–14 cal. ka (Figure 3a). Moreover, tuning of the uncorrected ^{14}C plateau ages to the well-defined ^{14}C age levels of atmospheric ^{14}C plateaus (op. cit.; vertical arrow in Figure S4a) provides local planktic ^{14}C reservoir ages of 300–450 years for the time span 17–14 cal. ka, corresponding to late H1 and Bølling, as compared with 900 years today and 1150 years prior to 17.5 cal. ka (i.e., during early H1 and LGM). On the basis of paired benthic-planktic ^{14}C ages, coeval apparent ventilation ages of LGM deepwater are extremely high, reaching ~3600–3800 years. After 17 cal. ka they decreased to ~2500 years, near 15 cal. ka to 2000 years, finally to 1400/1150 years at 14.3 cal. ka (Figure S4a).

[44] As in Core MD01-2416, the ^{14}C record of MD02-2489 reveals a distinct ^{14}C plateau which is tuned to the atmospheric plateau at 12.3 ^{14}C ka (14.2–14.9 cal. ka), implying a low planktic reservoir age of ~550 years versus 750 years today [*Southon and Fedje*, 2003]. 1000 years are inferred for a second ^{14}C plateau around 15.3–16.75 ka (Figure S4b), 1350 and 1700 years for plateaus near 17.1–17.5 and 17.9–18.6 cal. ka. The reduced reservoir ages near 14.5 cal. ka suggest that the short-lasting event of vertical mixing of surface waters at Site MD01-2416 may have extended over large parts of the subarctic North Pacific. Two aberrant ^{14}C ages (13.6, 13.8 ^{14}C ka) close to the core top reflect modern sediment distortion (Table 1 and Figure S2). Apparent ventilation ages of deepwater at Site MD01-2489 roughly parallel those at Site MD01-2416, but short-term dropped to 1600 years at 16.7 to 16.5 ka.

[45] To assign marine isotope stages (MIS) to the benthic δ^{18}O record of MD01-2416 for pre-LGM times (Figures 2–4b), we assumed a constant average difference of 1300 years between the reservoir ages of northwest Pacific surface and deepwater (900 years versus 2200 years today; *Southon et al.* [2005], *Schlosser et al.* [2001]). This implies that δ^{18}O signals of modern benthic foraminifera living at the sediment surface would record changes in global ice volume that actually would have occurred 1300 years ago. This is the time needed for a signal to spread from the source of North Atlantic Deepwater up to the far northern Pacific [*Duplessy et al.*, 1991b; *Sarnthein et al.*, 2005]. To account for this age difference the δ^{18}O records of *Uvigerina* spp. and *Cibicidoides* spp. were shifted downcore by 24 cm at Termination 1 (Figure 3a) and by 3–12 cm at terminations II–V (Figures 4a and 4b). This shift affects stable isotope records so that climate signals in planktic and benthic records occur almost in parallel. In reality, however, North Atlantic Deepwater signals of past changes in global ice volume reached the subarctic North Pacific during peak glacial times with a much larger lag of 2500 years versus δ^{18}O signals of surface water, a difference perforce here ignored [*Sarnthein et al.*, 2007]. The stable isotope records of *Cibicidoides* spp. in MD02-2489 were shifted downcore by 1600 years equivalent to 34 cm. However, benthic δ^{18}O excursions assigned to brinewater signals were excepted

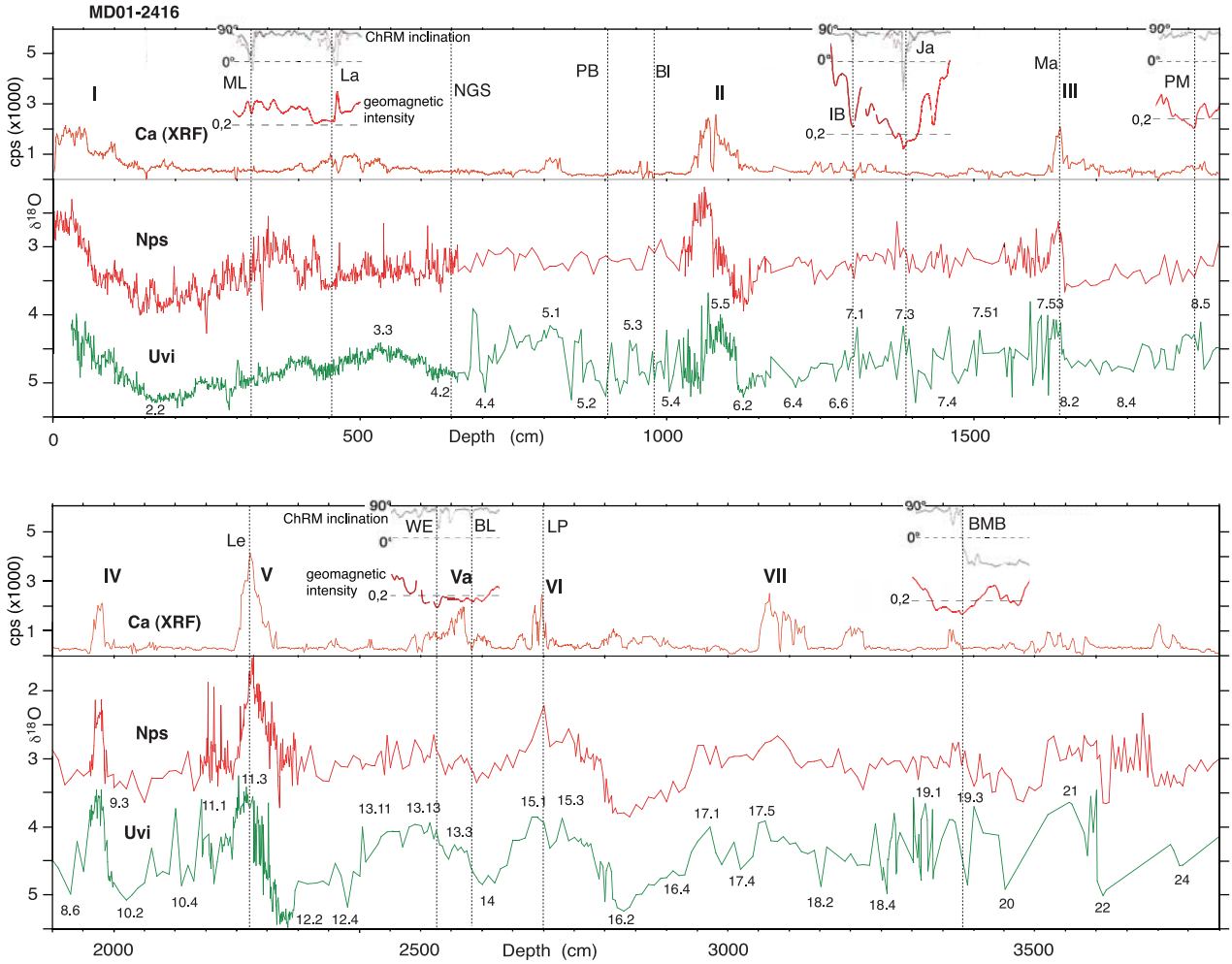

Figure 2. Planktic (Nps, *N. pachyderma* sin.) and benthic (Uvi, *Uvigerina* spp.) δ^{18}O stratigraphy and Ca (XRF) contents of the last 900 ka versus depth (cm bsf) in Core MD01-2416 from the subarctic northwestern Pacific (from *Sarnthein et al.* [2005], supplemented). Dotted vertical lines and names mark geomagnetic events, supplemented by selected examples of inclination changes 90° to <0° and coeval NRM/ARM-based magnetic paleointensity minima reaching to <0.2. The benthic δ^{18}O record is shifted downcore relative to the planktic δ^{18}O record to compensate for an average 1300-year difference in reservoir age between surface and deep waters. Decimal numbers at benthic δ^{18}O record are Marine Isotope Stages (MIS). Roman numerals are numbers of glacial terminations. BMB, Brunhes-Matuyama Boundary; LP, La Palma; BL, Big Lost; WE, West Eifel; Le, Levantine; PM, Portuguese Margin; Ma, Mamaku; Ja, Jamaica; IB, Icelandic Basin; Bl, Blake; PB, Post Blake; NGS, Norwegian Greenland Sea; La, Laschamp; ML, Mono Lake geomagnetic events.

from these shifts, because they originated at the sea surface, independent of deepwater age.

[46] The benthic δ^{18}O record of Core MD01-2416 stretches back to MIS 22 (Figure 2; definition of MIS after *Bassinot et al.* [1994] and *Sarnthein et al.* [2005], modified). In part, benthic and planktic δ^{18}O records show unusual oscillations such as those over parts of MIS 5 and 7. This makes them difficult to compare directly with records from elsewhere. Thus our initial definition of marine isotope stratigraphy was mainly based on the most positive excursions in benthic δ^{18}O near >4.5 and >5.0‰ PDB, since these values reflect culminations in global ice volume only, and hardly any other hydrographic factors, in contrast to negative δ^{18}O excursions that may contain local signals of brinewater and/or transient slight deepwater warming. For example, we ascribed the two apparently erratic δ^{18}O maxima on top of (well-defined) MIS 7.53–7.51 to MIS 7.4, and those on top of MIS 7.3–7.1 to MIS 6.6 and 6.4. The resulting suite of benthic MIS shows glacial-to-interglacial δ^{18}O shifts of 0.8‰ (Termination III) to 1.7‰ (Termination V), values that compare well with various estimates of changes in the global δ^{18}O ice effect. Also, the (depth-adjusted) suite was cross-checked with the suite of major excursions in planktic δ^{18}O, which

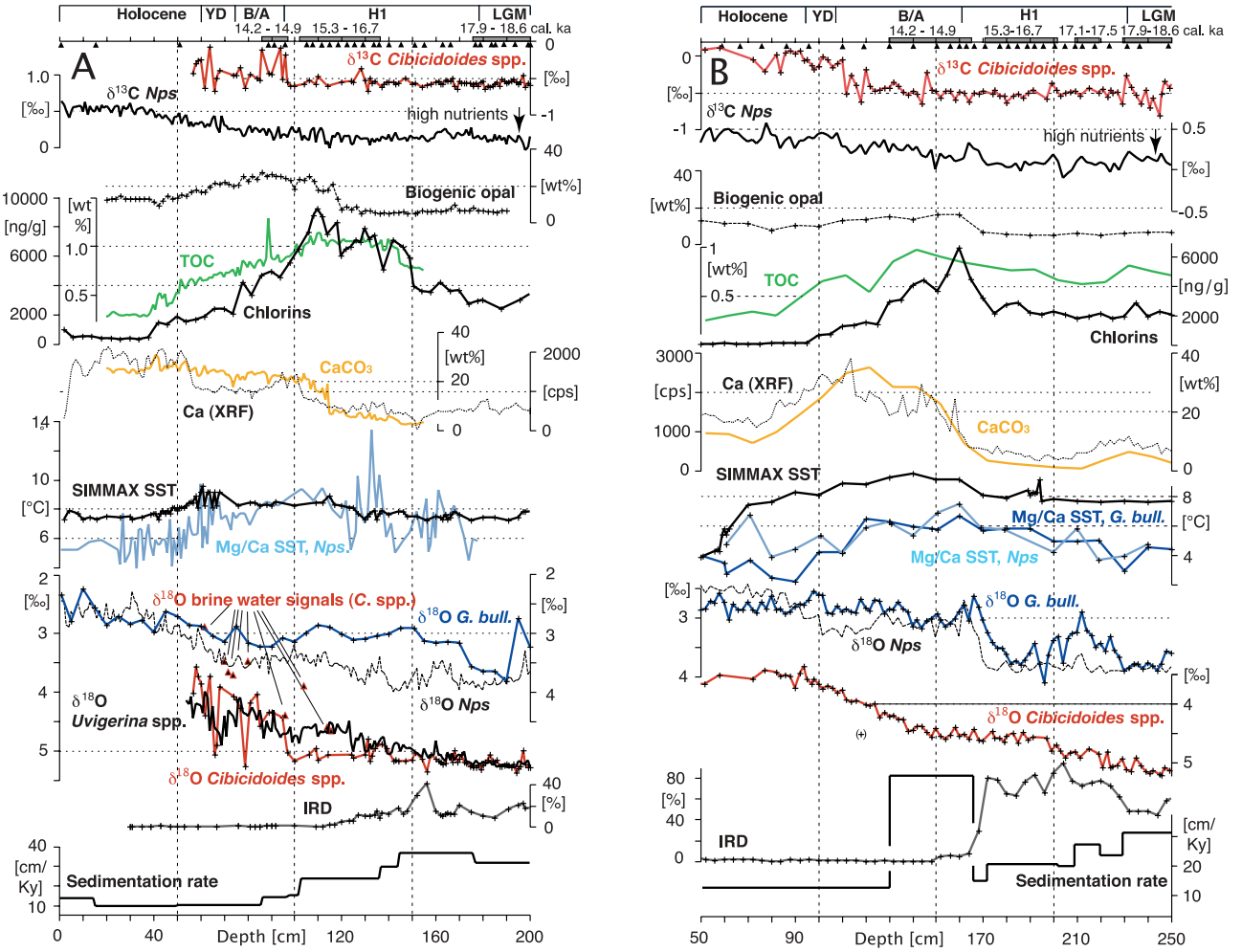

Figure 3. Paleoceanographic records from the (a) western (MD01-2416) and (b) eastern (MD02-2489) subarctic North Pacific for Termination I and the Holocene. Records include paired surface (*G. bull*., *G. bulloides*), subsurface (Nps, *N. pachyderma* sin.), and bottom water (*Uvigerina* and *Cibicidoides* spp.) stable isotope signals (uncorr.), and sediment tracers of paleoproductivity (biogenic opal; chlorins; TOC, total organic carbon). XRF, X-ray flourescence; cps, counts per second; SIMMAX SST, sea surface temperature estimates for summer, based on planktic foraminifera census counts, and Mg/Ca-based SST for early (*N. pachyderma* sin.) and late summer (*G. bulloides*); IRD, ice-rafted debris. Carbon 14 plateaus and age control (arrow heads and bold bars above top panel) for MD01-2416 after *Sarnthein et al.* [2007], ^{14}C plateaus and age control for MD02-2489 based on ^{14}C dates listed in Table 1. Note that δ^{18}O and δ^{13}C (‰ PDB) records for *Cibicidoides* spp. (*C.* spp.) and *Uvigerina* spp. are shifted downcore by 24 cm (MD01-2416) and 34 cm (MD02-2489) to account for a minimum offset of 1300 and 1600 years, respectively, between planktic and benthic stable isotope records. In contrast, benthic brinewater signals of *Cibicidoides* spp. display surface water processes and thus retain original core depths. North Atlantic stratigraphic terms (YD, Younger Dryas; B/A, Bølling-Allerød; H1, LGM, Last Glacial Maximum) are shown for stratigraphic comparison at figure top. No isotope record of *Uvigerina* spp. was established for MD02-2489 because of insufficient specimens.

equally are subject to changes in global ice effect. However, the two δ^{18}O records don't match over several core sections (Figure 2), supposedly because of major changes in SST and SSS.

[47] Age control of the sediment section 250–2950 cm bsf in Core MD02-2489 was based on a high-resolution planktic stable isotope record only (Table 2), covering the last 90 ka.

[48] Important independent evidence to confirm or disprove our MIS stratigraphy in MD01-2416 came from the suite of short-term events of minimum magnetic paleointensity (NRM/ARM), several of them being linked to reversed or less steep inclination (Table 3 and Figure S3). These magnetostratigraphic tie points were tuned to stacked records of changes in the global geomagnetic field, that have been age-calibrated by *Guyodo and Valet* [1999],

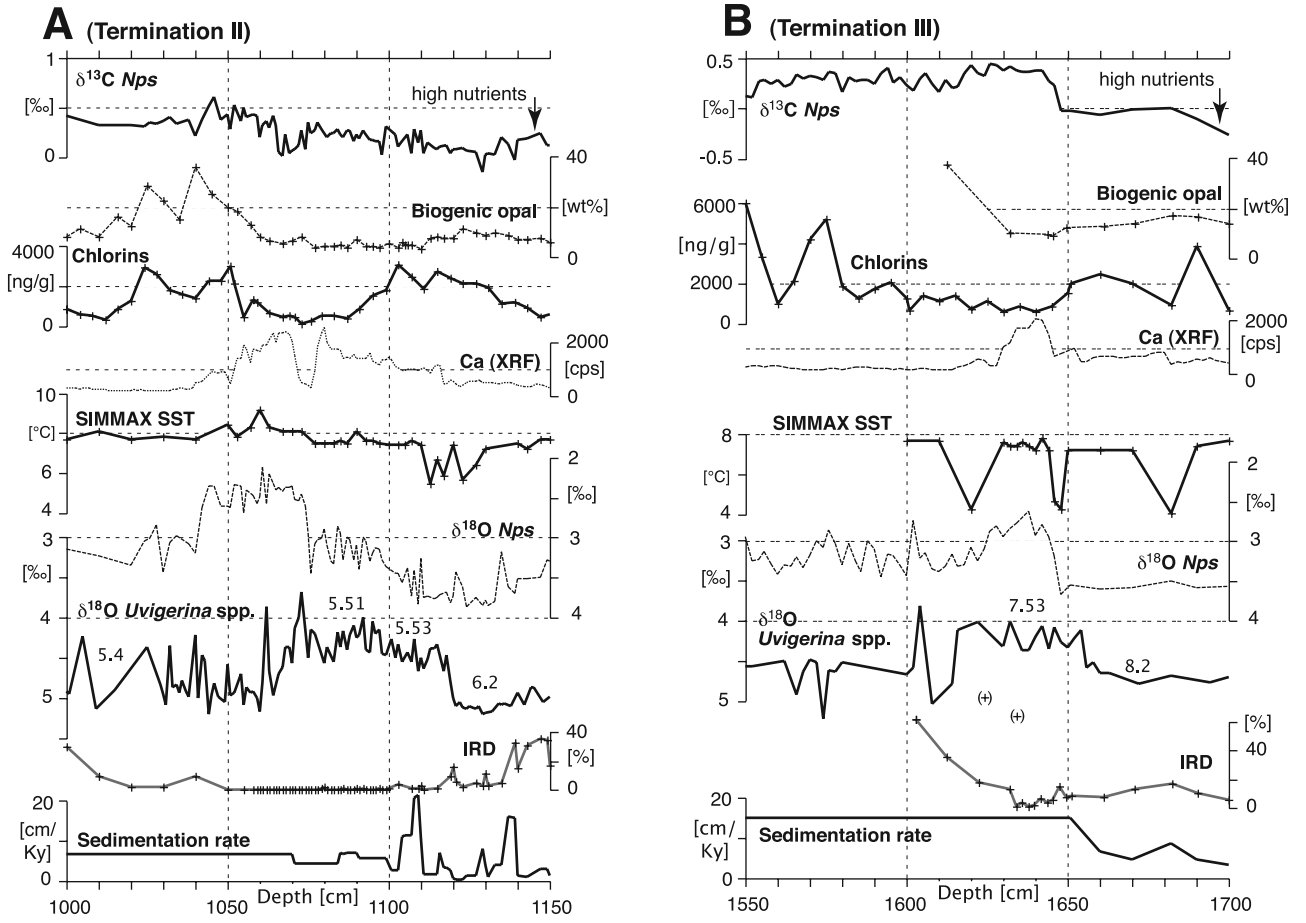

Figure 4a. Paleoceanographic and sediment records for Termination II–III at Site MD01-2416. Explanations of proxies as for Figure 3; numbers along benthic $\delta^{18}O$ record indicate marine isotope stages. To account for an average 1300-year minimum offset between planktic and benthic stable isotope records the $\delta^{18}O$ record for *Uvigerina* spp. is shifted downcore (a) by 5 cm at Termination II and (b) by 12 cm at Termination III.

Singer et al. [2002, 2005], and *Thouveny et al.* [2004]. Age uncertainties in part stem from the length of these intervals, in part from divergent definitions. Geomagnetic events were crucial for defining controversial positions of MIS 3, 7.3–7.1, 8.5, 11.3, 13–14, and 19 near the Brunhes-Matuyama Boundary (Figures 2 and S3). Simple dash-dotted lines in Figure 2 show further age-calibrated events of minimum geomagnetic intensity. Our age model, based on joint geomagnetic and $\delta^{18}O$ evidence, identifies MIS 7.5–6.4 and other stages at core depths that deviate significantly from the age model of *Galbraith et al.* [2008] for the same core, derived from minimum tuning to glacial terminations I to V.

[49] After correlating geomagnetic events, small-scale features in the benthic $\delta^{18}O$ record of MD01-2416 were tuned to substage features in the stacked high-resolution planktic $\delta^{18}O$ record of *Bassinot et al.* [1994], using the AnalySeries-1.2 program for a detailed visual correlation of minor $\delta^{18}O$ excursions [*Paillard et al.*, 1996]. In total, our age model resulted in age uncertainties of ~3500 years for major MIS and substages (named with one decimal; e.g., glacial terminations, peak cold stages as 4.2, 6.2–6.6, end of MIS 7.4, etc.). This uncertainty won't exceed significantly the range assumed for records with direct orbital tuning. In contrast, minor substages (named with second decimals; e.g., MIS 7.51) have relative age uncertainties which generally exceed the age differences in between two of these substages, hence may lead to spurious sedimentation rates.

[50] Spectral analysis of the benthic $\delta^{18}O$ record in MD01-2416 validates our age model. Such analysis reveals a well-focused sequence of 95/41/23/19-thousand year periods (initial version depicted by *Sarnthein et al.* [2005]). The spectra gained in focus with each step of refining age control. The planktic record shows a dominant 97,000-year and very minor 40,000-year period; spectral analysis of Ca intensity a single prominent period of 95,000 years (only for the last 550 ka). This period reflects most prominent $CaCO_3$ spikes at peak interglacials (Figures 2 and 5a) and is confirmed by the data of *Jaccard et al.* [2005] for neighbor ODP Site 882.

[51] Mass accumulation rates (AR) were derived for sediment sections of terminations I to V. This was accomplished using sedimentation rates linearly interpolated be-

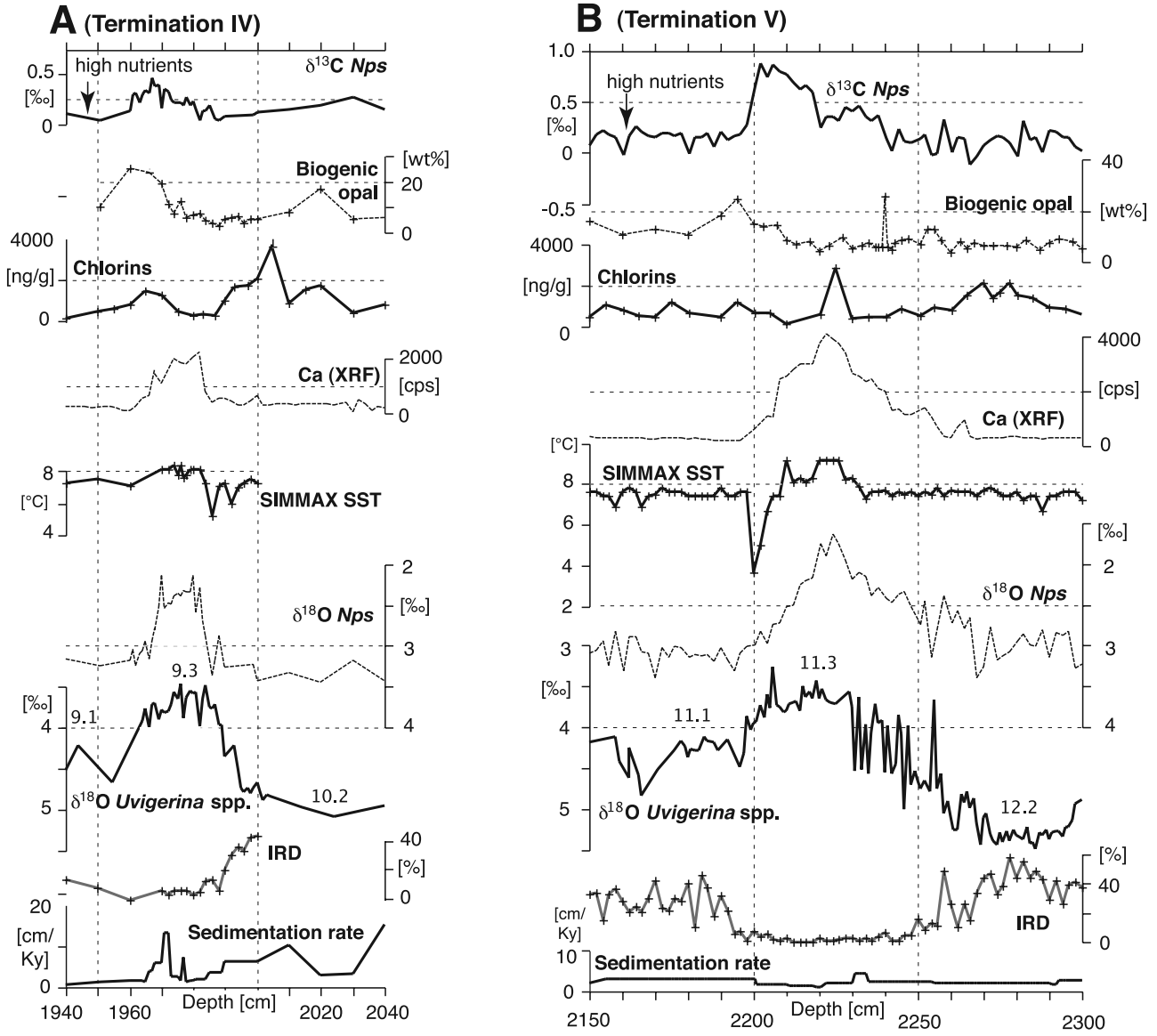

Figure 4b. Paleoceanographic and sediment records for Termination IV–V at Site MD01-2416. Explanations of proxies as for Figure 3; numbers along benthic $\delta^{18}O$ record indicate marine isotope stages. To account for an average 1300-year minimum offset between planktic and benthic stable isotope records the $\delta^{18}O$ record for *Uvigerina* spp. is shifted downcore (a) by 4 cm at Termination IV and (b) by 3 cm at Termination V.

tween depth/age control points of major substages, dry-bulk density data (http://www.pangaea.de), and weight % of the sediment components under discussion. Sampling resolution was also controlled by our age model resulting in differential (in part, apparent) sedimentation rates, and by variable sample spacings, as listed for various proxies in Table 2.

4. Results

4.1. Termination I in the Northwestern Pacific (Core MD01-2416)

[52] The ^{14}C reservoir ages of surface waters form a good tracer of vertical mixing in the surface ocean. They decreased during early deglacial times, 17.5–14.5 ka (Figure S4a; 170–90 cm bsf), from 1150 to 300–450 years, as compared to 900 years today. At the same time, apparent deep water ventilation ages dropped from 3600–3800 years to <1400 years [*Sarnthein et al.*, 2007]. The age reduction reflects major vertical mixing of surface waters in the subarctic northwestern Pacific after ~17 cal. ka, and was coupled to short-lasting but important deepwater convection. In total, the deglacial regime was similar to that in the modern northern North Atlantic.

[53] Enhanced vertical mixing of surface waters after 15 cal. ka is also supported by only very minor deviations between paired $\delta^{18}O$ records of *G. bulloides* and *N. pachyderma* sin., amounting to 0.25‰ and less (Figure 3a). In contrast, preceding $\delta^{18}O$ deviations reached 0.5–1.0‰

Table 3. Events of Paleomagnetic Intensity Minima and Changes in Magnetic Inclination Measured in Core MD01-2416[a]

Reversal/Event/Excursion	Quality of Magnetic Signals	Paleomagnetic Intensity Minimum			Magnetic Inclination Reversal (mbsf)	Age of Geomagnetic Event (ka)
		Top depth (mbsf)	Bottom depth (mbsf)	Mean depth (mbsf)		
Mono Lake	1	3.21	3.32	3.27	3.23	28.4
Laschamp	1	4.40	4.64	4.58	4.55	41
Norwegian-Greenland Sea	2	6.50	6.56	6.53	-	65
Post Blake	2	8.95	9.44	9.05	-	94
Blake	2	10.30	10.71	10.45	-	115
Icelandic Basin	1	12.90	13.10	13.02	13.00	184
Jamaica	1	13.81	14.04	13.85	13.85	212
Mamaku	2	16.30	16.66	16.44	-	246
Portuguese Margin	2	18.36	18.55	18.58	(?18.75)	285 (?287)
Levatine	2	22.11	22.34	22.19	-	410
West Eifel	2	25.25	25.29	25.27	25.25	504
Big Lost (?)	2	25.44	25.85	25.68	25.85	530
La Palma	2	28.06	28.11	28.06	-	622
B/M Boundary	1	33.61	34.01	33.82	33.81	789

[a]See Figure 2. Quality of events: (1) characteristic remanent magnetization inclination change and paleointensity minimum; (2) paleointensity minimum only. Ages of events are compiled from *Thouveny et al.* [2004] and *Singer et al.* [2002, 2005].

from 18–15 cal. ka (coeval with H1), then reflecting pronounced stratification of surface waters, except for three distinct precursor pulses of invigorated vertical mixing ~17.5, ~16.5, and ~15.5 ka. This mixing is shown by both short-lasting minima in planktic $\delta^{18}O$ deviation (<0.5‰; near 170, 135, 110 cm bsf) and short periods of pronounced 4–6°C increase in Mg/Ca-based subsurface temperatures. SIMMAX-based SST do not reveal these pulses but a gradual, smooth rise by 2°C, reaching a first maximum after 16 cal. ka and a second, slightly higher peak at 12.0–11.5 cal. ka (during the late Younger Dryas), coeval with a further Mg/Ca-based maximum in subsurface SST.

[54] Alternating times of surface water stratification and vertical mixing during the early deglacial (17.0–14.5 cal. ka) coincided with a prominent overall productivity maximum. In sediments between 150 and 90 cm bsf, TOC peaks of >1% then coincided with chlorin contents that reached > 9000 ng g^{-1}, in contrast to ~2500 ng g^{-1} near 17.5 cal. ka, the end of abundant IRD and the intensive surface water stratification characteristic of LGM times. After ~15 cal. ka (coeval with the onset of B/A), TOC and chlorin-based productivity estimates decreased remarkably down to <1000 ng g^{-1} in the early Holocene. Contents of biogenic opal, our second productivity proxy, jumped abruptly from 5 to 25 wt% near 16 cal. ka (~118 cm bsf), thereby confirming the chlorin-based productivity high, but lagging behind it by ~1100 years. Likewise, the decline of opal lagged behind that of chlorins by almost 2000 years (in harmony with *Keigwin et al.* [1992]). Accordingly, sedimentation rates (Figure 3a) were two to four times higher during early deglacial than during late-deglacial-to-Holocene times, first because of IRD input (30–36 cm/1000 years), and later because of maximum algal (chlorins and diatoms) productivity and pelagic sediment flux (23 cm/1000 years). When productivity and pelagic sediment flux declined after 14 cal. ka, sedimentation rates dropped to 15 and 10 cm/1000 years. In contrast, reduced $CaCO_3$ dissolution did not result in enhanced bulk sedimentation rates in the early Holocene.

[55] In general, high surface water productivity went along with high nutrient concentrations in subsurface waters, as depicted by minimum $\delta^{13}C$ values of *N. pachyderma* sin. (0–0.2‰ uncorr.), and vice versa, low productivity coincided with high $\delta^{13}C$ values of *N. pachyderma* sin. (0.6–1.45‰ for DIC). Accordingly, nutrient depletion has affected both surface and subsurface waters, documenting a well-mixed surface ocean after 15 cal. ka. This is in harmony with low ^{14}C reservoir ages and minimum $\delta^{18}O$ deviations between the paired surface and subsurface records of *G. bulloides* and *N. pachyderma* sin.

[56] The prominent $CaCO_3$ maximum marking late Termination I and early MIS 1 (Figures 2 and 3a) is mostly unrelated to changes in overall paleoproductivity. Carbonate content starts to rise near 115 cm bsf (~15.8–15.3 cal. ka; late H1), coeval with the rise in biogenic opal (*nb.* the apparently delayed rise in Ca intensities results from analytical artifacts of XRF analyses outlined previously). This initial increase in Ca well before to the main $CaCO_3$ high, may signify enhanced carbonate flux because required SST exceeded a minimum level to increase coccolith productivity. However, the main peak in $CaCO_3$ and Ca contents only occured at 55–5 cm bsf (~9.8 to 6.0 cal. ka), approximately 6000–8000 years after the chlorin- and opal-based productivity maxima of Termination I. The depositional regime of the early Holocene carbonate maximum may be inferred, by comparison with the clear $\delta^{13}C$ rise of epibenthic *Cibicidoides* spp. by 0.5% after 15 cal. ka. The rise likewise documents higher bottom water ventilation and a rapid drop in TOC flux (as reflected by the productivity records), leading to a reduction of organic fluff on the sea floor [*Sarnthein et al.*, 1994; *Mackensen et al.*, 1993]. Both factors provide optimum conditions for $CaCO_3$ preservation.

[57] In summary, the Termination I to early Holocene section of MD01-2416 documents a clear suite of productivity oscillations: (1) maxima in chlorins and TOC that were followed by (2) a maximum in biogenic opal and (3) a peak of $CaCO_3$, a complex result of both enhanced $CaCO_3$ flux and, especially, low $CaCO_3$ dissolution on the seafloor. After 16 cal. ka, in particular after 14.5 cal ka the great rejuvenation of bottom water (Figure S4a) was crucial for increased $CaCO_3$ content, since it led to significantly higher

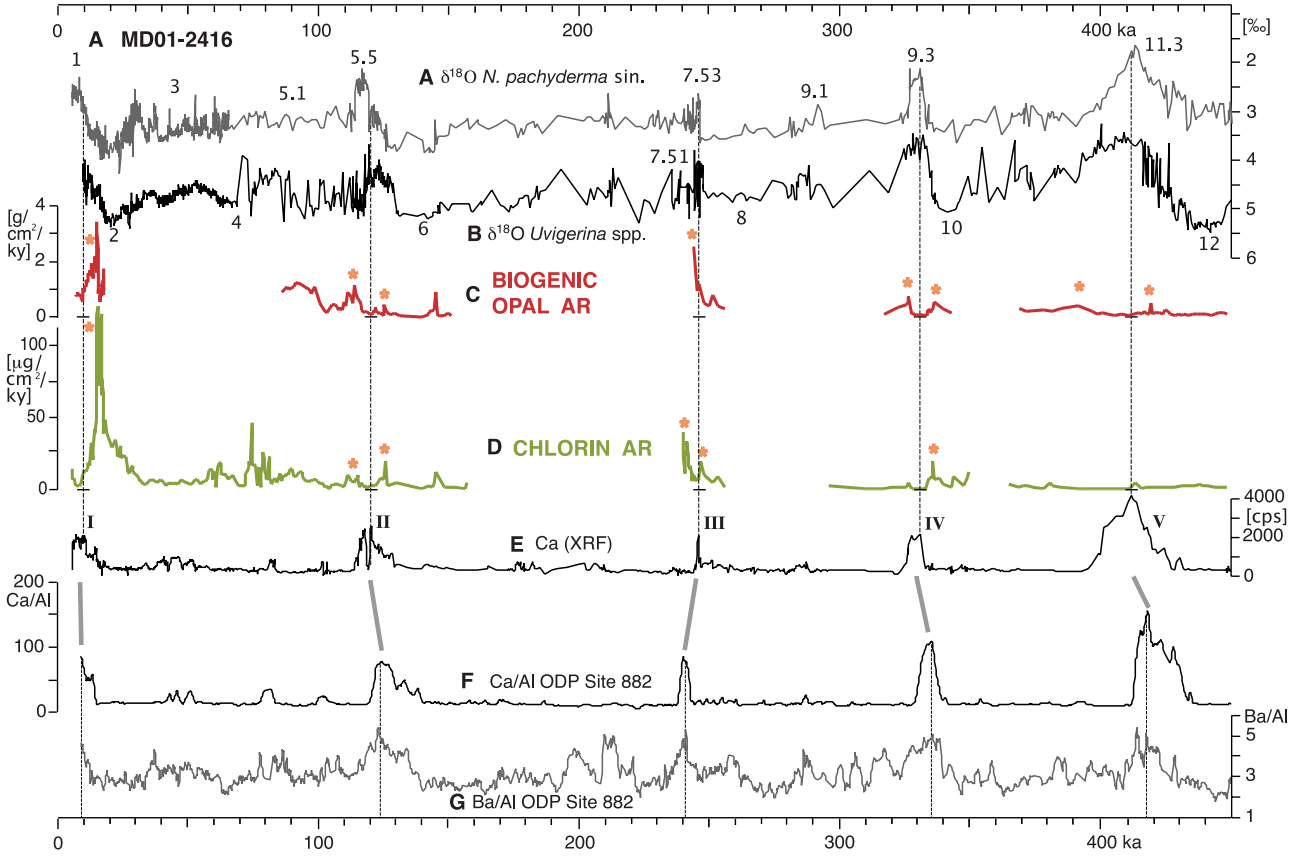

Figure 5a. Accumulation rates (AR) of chlorines and biogenic opal showing productivity maxima prior and subsequent to peak interglacials, marked by asterisks, versus maxima in $CaCO_3$ preservation, marine isotope stratigraphy, and age (ka) at Site MD01-2416. Roman numerals at Ca peaks mark terminations I to V. The $\delta^{18}O$ record of *Uvigerina* spp. is shifted 1300 years downcore to account for the average minimum offset between planktic (a) and benthic (b) stable isotope records. Vertical dashed lines highlight positions of early interglacial Ca maxima. Maxima in Ba/Al [*Jaccard et al.*, 2005] match short-term peaks of Ca and $CaCO_3$, used for chronostratigraphic tuning of neighbor sites 882 and MD01-2416 (e–g) and thus are coeval with biogenic opal and chlorin records of minimum productivity (c and d). Chronology for Site 882 is based on tuning to Vostok ice core record [*EPICA Community Members*, 2004] and the assumption of largely constant sedimentation rates [*Galbraith et al.*, 2008].

bottom water ventilation, and hence highly improved $CaCO_3$ preservation, until the mid Holocene (~6 cal. ka.).

4.2. Termination I in the Northeastern Pacific (Core MD02-2489)

[58] The records of cores MD02-2489 and MD01-2416 have a lot of paleoceanographic and paleoproductivity features in common. Differences may be linked to the influence of the Aleutian Current on sedimentation at northeast Pacific Site MD02-2489. Coeval with the northwest Pacific ^{14}C reservoir ages of surface water dropped from 1700 years prior to 18 cal. ka to a minimum of 550 years near 14.9–14.2 cal. ka, indicating that vertical mixing of surface waters intensified during late Termination I (Table 1 and Figure S4b). This conclusion is corroborated by minimum offsets between paired $\delta^{18}O$ and Mg/Ca records of surface (*G. bulloides*) and subsurface waters (*N. pachyderma* sin.), except for a short-lasting 1.5‰ offset near 17–18 cal. ka (200–230 cm bsf), a bioturbation-induced lead of surface water signals near ~15 cal. ka, and an unexpected negative signal departure of 0.3‰ around 14.0–11.5 cal. ka (coeval with Allerød and Younger Dryas). The latter is possibly a result of strong seasonality [*Asahi and Takahashi*, 2007] and vertical stratification.

[59] Deglacial IRD input at northeast Pacific Site MD02-2489 was 2–3 times greater than at Site MD01-2416 near 19–15 ka and decreased abruptly 1500 years later, near the end of H1, than at Site MD01-2416. Accordingly, the deglacial evolution of iceberg sources was different in the two regions.

[60] The drop in IRD at ~15 cal. ka matches a weak 1–1.5°C increase of SST at ~170 cm bsf in all three SST records for surface and subsurface waters (Figure 3b). Precursor warmings, where SSTs were rising by 2–3°C, occur near 220 and 195 cm bsf, possibly coeval with the major SST warmings found at Site MD01-2416 near 17.5 and 16.5 cal. ka. All SST records at Site MD02-2489 culminated around 14.9–14.2 cal. ka, different from northwestern Site

MD01-2416, where SST culminated only near 11.5 cal. ka. Over late Termination I and the earliest Holocene Mg/Ca-based SST of surface waters dropped sharply by ~4°C at ~14–11 cal. ka (120–90 cm bsf). Subsurface SST and SIMMAX-based SST decreased much later, after ~11 cal. ka (90–50 cm bsf).

[61] Unlike MD01-2416, the great deglacial drop in IRD coincided with a prominent and abrupt decrease in SSS near 15.3 cal. ka (160–180 cm bsf). In surface waters it started with a 1.15‰ decrease in δ^{18}O of *G. bulloides* (Figure 3b). This amount is equal to >1 psu SSS, when taking into account the coeval SST increase corresponding to <0.3‰ and a reduction in global ice effect of 0.3‰. In subsurface waters a more or less coeval decline in SSS can be inferred from a 1‰ decrease in δ^{18}O of *N. pachyderma* sin. only 7 cm further upcore, which suggests good vertical mixing of the surface ocean (the apparent lag of signals may simply result from reversed vectors of bioturbational mixing of "warm" and "cold" species in deglacial sediment sections).

[62] Together with deglacial warming and the distinct SSS drop, both chlorin content (rising from 2100 to 6600 ng g^{-1}) and biogenic opal (rising from 6 to 16 wt%) indicate a massive rise in productivity near 15.3–14.7 cal. ka (170 cm bsf; i.e., during final H1), right near the end of IRD deposition. This rise occurred >2000 years later than in the northwest Pacific and only little prior to a "green sediment layer" and opal-based productivity peak in the Bering Sea (Core JPC17; *Brunelle et al.* [2007]), where productivity changes may also be controlled by variations in the Aleutian Current. Sedimentation rates at MD02-2489 culminated at 50 cm/1000 years (Figures 3b and S4b), as compared to 15–30 cm/1000 years during earlier and later periods. As in the northwest Pacific, the chlorins decreased significantly after 14.5 cal. ka, TOC with a lag of 500 to 1500 years, whereas biogenic opal decreased only a little and gradually until the early Holocene.

[63] Coeval with the chlorin drop, the δ^{13}C-based nutrient record of *N. pachyderma* sin. for subsurface waters increased from 0.0 to 0.5‰ (uncorr.) between 150 and 100 cm bsf (~14.5–12.0 cal. ka). Thus we infer a decrease in nutrients that affected both subsurface and surface waters. Decreasing nutrients in surface waters are also suggested by the end of vertical mixing, as documented by the onset of distinct deviations between paired δ^{18}O records of *N. pachyderma* sin. and *G. bulloides* (Figure 3b).

[64] The outlined decrease in nutrients and productivity coincided with XRF-based values of Ca that increased from 500 to almost 3000 cps (50% higher than in Core MD01-2416) and $CaCO_3$ contents that increased from zero to 35% after 14 cal. ka (120 cm bsf). Accordingly, the prominent Ca maximum was linked to reduced organic fluff and bottom water corrosivity at the sea floor, as at Site MD01-2416.

4.3. Terminations II–V in the Northwest Pacific (Core MD01-2416)

[65] In many aspects the sediment records across glacial terminations II–V and subsequent peak interglacials, MIS 5.5, 7.5, 9.3, and 11.3, closely resemble the trends established for Termination I (Figures 4a and 4b).

[66] As with early Termination I, glacial IRD deposition in the northwestern Pacific ended with an extremely short (century-scale) but distinct IRD maximum near the onset of terminations II, IV, and V, and a very minor peak at Termination III. IRD was also abundant during the "aborted" short glacial of MIS 7.4. Terminations IV and V started with an abrupt drop in IRD, whereas hardly any IRD was deposited prior to terminations II and III, that is during peak glacial MIS 6.2 and 8.2. Obviously, different glacial stages had different patterns of iceberg drift and abundance.

[67] In this study, IRD and SIMMAX-based SST, in conjunction with planktic δ^{18}O of *N. pachyderma* sin., provide the major records of paleohydrographic changes affecting terminations II to V. Most obvious are major but short-lasting summer coolings by 2–4°C near the end of IRD deposition and the onset of terminations II, III, and IV (Figures 4a and 4b). These coolings are interpreted by analogy to Mg/Ca-based SST coolings of subsurface waters during Termination I and MIS 1 (Figure 3a), where paired planktic δ^{18}O records of surface water stratification and reconstructions of short-term changes in ^{14}C reservoir ages of surface and deepwater provide much clearer insights into the general paleoceanographic setting. Thus we regard the striking coolings as a record of short-term pulsating oceanographic conditions similar to those during early Termination I, in particular as record of short periods of vertical mixing of the surface ocean and of deepwater convection in the subarctic northwest Pacific. For unknown reasons, Termination V shows almost constant SST reaching far back into glacial MIS 12.2; hence it forms an exception to the rule of early deglacial SST oscillations.

[68] Later on, during peak interglacials MIS 5.5, MIS 7.53, 9.3, and 11.3, coeval with the outstanding maxima of Ca intensity, SST exceeded the average level by about 1–2°C for a short period, like during the earliest MIS 1. Subsequently, the end of interglacial stages 11.3 and 7.53 reveals a dramatic, but short-lasting SST drop of up to 5.5°C, a shift supported by an equivalent increase in planktic δ^{18}O values of *N. pachyderma* sin. This SST drop is not seen at the end of MIS 9.3 and 5.5, a consequence of too low sampling resolution (left side of Figures 4b and 4a).

[69] Late glacial stages and the initial part of all terminations are characterized by extreme lows in planktic δ^{13}C of *N. pachyderma* sin. (0 to −0.3‰), a proxy of high macronutrient concentrations in subsurface waters, and approximately coeval with the striking excursions of low SST. In contrast, clear planktic δ^{13}C maxima (up to 0.8–1.7‰ for DIC during MIS 11.3) document phases of major nutrient depletion during (late) peak interglacials. They were followed by an abrupt recovery of the nutrient budget right at the end of interglacials, for example at MIS 11.3 and 9.3, and during the course of MIS 5.5–5.4, but not for MIS 7.5.

[70] High nutrient concentrations in subsurface waters near the onset of terminations II–V were linked to prominent maxima of chlorins (2000 to 4000 ng g^{-1}), a proxy for algal productivity. Nevertheless, these chlorin spikes did not reach the extreme level found for early Termination I (8,000–10,000 ng g^{-1}; Figure 3a), perhaps a result of diagenesis. Subsequent nutrient depletion resulted in coeval

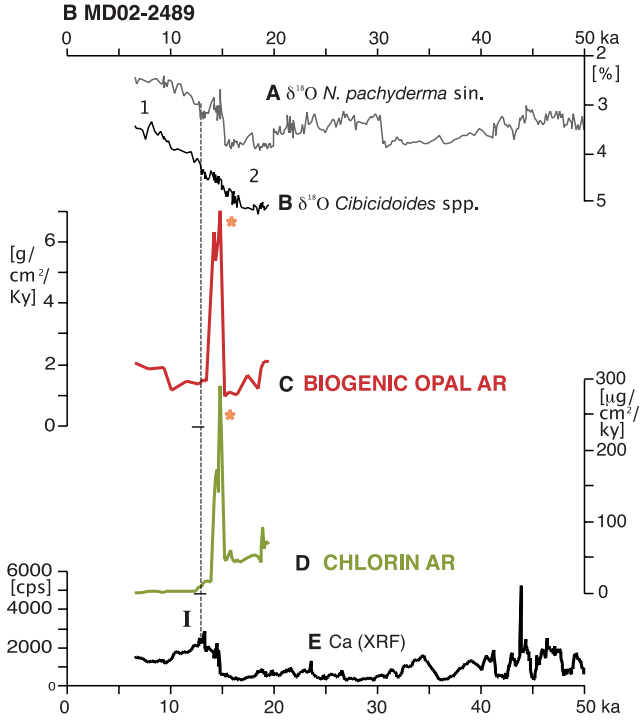

Figure 5b. Accumulation rates (AR) of chlorines and biogenic opal showing productivity maxima prior and subsequent to peak interglacials, marked by asterisks, versus maxima in $CaCO_3$ preservation, marine isotope stratigraphy, and age (ka) at Site MD02-2489. Roman numeral at Ca peak marks Termination I. The $\delta^{18}O$ record of *Cibicidoides* spp. is shifted 1.6 ka downcore to account for the average minimum offset between planktic and benthic stable isotope records. Vertical dashed line highlights position of early interglacial Ca maximum.

minima of chlorin productivity during peak interglacial stages. A second group of high chlorin values marks the immediate end of interglacial stages: it was sometimes more pronounced than the preceding deglacial chlorin maxima (e.g., 6000 ng g^{-1} after MIS 7.5), and sometimes equally or less pronounced (e.g., after MIS 5.4 and 9.3). Unlike the pattern at early terminations, various chlorin maxima subsequent to interglacials are not associated with coeval maxima of subsurface nutrients, possibly the result of enhanced surface water stratification. The origin of a single, particularly high value of chlorin concentration in MIS 11.3 is not clear.

[71] Unlike the biogenic opal maximum at Termination I, no other termination reveals any such productivity maximum. On the other hand, significant spikes of 25 wt% (early MIS 11.2 and 9.2) to 38 wt% (early MIS 7.52 and 5.4) mark the end of peak interglacial stages. Each of these opal maxima coincides with a second maximum in chlorin percentage and accumulation rates (Figure 5a) during early cold MIS 5.4 and 9.2, but not during MIS 7.52 and 11.2.

[72] As during MIS 1, outstanding Ca maxima occur in all peak interglacial stages over the last 500 ka. Ca values rise from approx. 400 to >2100 cps at interglacials MIS 5.5 (double peak), 7.53, and 9.3, and to 4100 cps at MIS 11.3; this is an order of magnitude above the general background level. These peaks are coeval with minima in TOC fluff, and nutrients in subsurface waters as recorded by AR of chlorins and biogenic opal (Figure 5a) and $\delta^{13}C$ of *N. pachyderma* sin. Accordingly, and as stated for Termination I, Ca spikes are anticorrelated to productivity and have resulted from optimum $CaCO_3$ preservation near 2300-m water depth during peak interglacial times.

5. Discussion

[73] Various processes control changes in nutrient inventories and algal productivity in the open subarctic North Pacific. These changes do not necessarily match those in the Okhotsk and Bering adjacent seas [*Sato et al.*, 2002; *Brunelle et al.*, 2007]. Vertical mixing of oligotrophic surface water with nutrient-enriched waters from below is most important. During late to present Holocene times this nutrient source appears to be largely barred by almost stable stratification of subpolar waters [*Clarke et al.*, 2001; *Sarnthein et al.*, 2004], even more so during the last glacial [*Keigwin et al.*, 1992]. Nevertheless, despite stratification, the modern pycnocline appears to tap directly into nutrient-rich waters from the deep ocean, in particular Pacific Deepwater upwelled in the northwestern North Pacific [*Tsunogai*, 2002; *Sarmiento et al.*, 2004]. This tapping is also suggested by extremely high ^{14}C reservoir ages of 900 years in modern surface waters [*Southon et al.*, 2005] and may support the intense plankton productivity found all over the subarctic North Pacific. In addition, the nutrient pool in high-latitude surface waters is recharged by vigorous vertical mixing during winter, whereas high freshwater supply and temperatures support a stabile pycnocline during summer [*Roden*, 1995].

[74] The supply of silica, a limiting factor to diatom productivity, does not follow a linear relationship with N and P [*Yool and Tyrrell*, 2003] and thus generates productivity records of biogenic opal that differ somewhat from those of chlorin and TOC. In part, this is a result of slower dissolution of silica particles. In addition, specific SiO_2 sources such as fluvial input from the Rocky Mountains and Coastal Ranges in Canada and the USA, may be particularly important along the eastern North Pacific margin, where the low-salinity Aleutian Current contributes significantly to the near-surface nutrient inventory. This current may be less important for diatom growth in the far northwestern Pacific, even though a western branch of the Aleutian Current today reaches all the way up to Site MD01-2416 (traced by plastic toys; *Ebbesmeyer et al.* [2007]). In addition, wind-borne iron forms a limiting trace nutrient [*Tsuda et al.*, 2003] that may have strongly increased during glacial and early deglacial times.

[75] As summarized in Figures 5a and 5b, North Pacific regimes of productivity and sedimentation were subject to complex variations over the last 450 ka, whereas changes in $CaCO_3$ followed a simple bimodal pattern [*Jaccard et al.*, 2005; *Sarnthein et al.*, 2005]. To disentangle the structure and complex forcings of these divergent pattern: (1) We try to unravel processes controlling the deglacial-to-interglacial

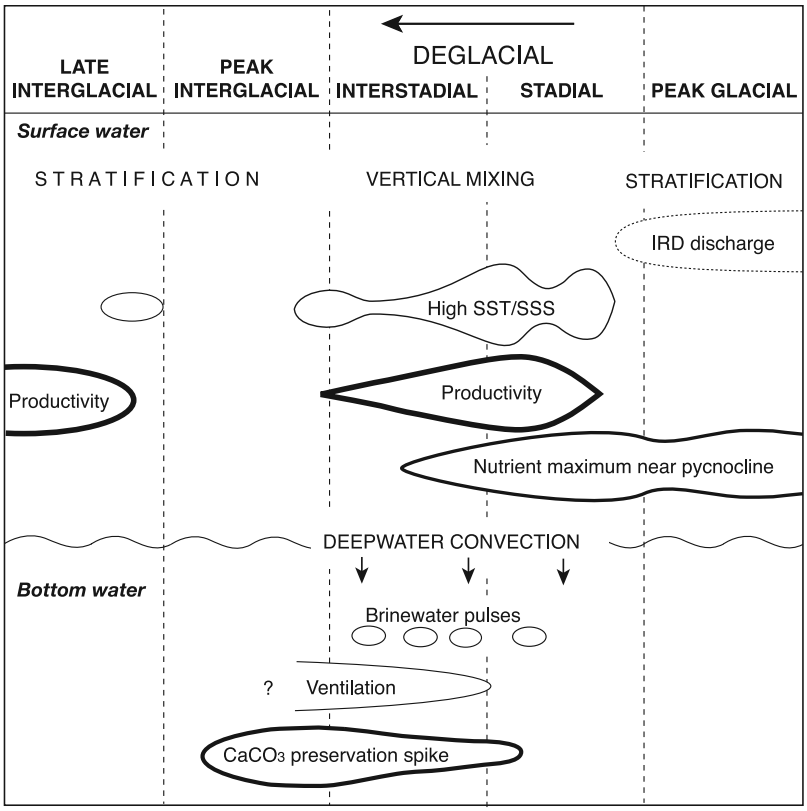

Figure 6. Summary scheme of changing paleoceanographic regimes in the subarctic northwest Pacific over interglacial stages MIS 1, 5, 7, 9, and 11. Paleoproductivity estimates derived from accumulation rates of chlorin and biogenic opal culminating during both deglacial and late interglacial times. Subsurface nutrients near the pycnocline are deduced from δ^{13}C of *N. pachyderma* sin. Stratification and vertical mixing of surface waters are inferred from (1) planktic stable isotope differences between surface dweller *G. bulloides* and subsurface dweller *N. pachyderma* sin. and (2) planktic ^{14}C reservoir ages for Termination I. Sea surface temperature (SST) estimates are based on Mg/Ca values of *N. pachyderma* sin. and SIMMAX estimates. Sea surface salinity (SSS) is estimated from ice volume-corrected and SST-corrected planktic δ^{18}O records. IRD is ice-rafted debris. Brinewater pulses are inferred from extremely negative δ^{18}O excursions of epibenthic *Cibicidoides* spp., bottom water ventilation from its δ^{13}C values.

hydrography of glacial Termination I, where paleoceanographic processes are best documented by ^{14}C paleowater mass ages [*Sarnthein et al.*, 2007] and other proxies. (2) We extract and interpret a standard series (Figure 6) of short-term events of nutrient enrichment and productivity increase in the context of the scenarios defined for Termination I. (3) We trace this standard sequence over terminations II–V and subsequent interglacials MIS 5.5 to MIS 11 on the basis of our multiproxy records. (4) We speculate on implications for deglacial events of short-term major CO_2 release from the deep North Pacific.

5.1. Changes in Hydrography Over Termination I and MIS 1

[76] Unlike the northern North Atlantic with 2.5–4.0°C [*Pflaumann et al.*, 2003], the open subarctic northwest Pacific had maximum summer SSTs of 4–8°C over the Last Glacial Maximum (Figure 3). Thus sea ice was absent during the summer and possibly also during winter [*CLIMAP Project Members*, 1981]. Although glacial sea ice hardly limited the growing season in this region, ice rafting and iceberg melting did occur, which led to stratified surface waters in the subpolar gyre. This is evidenced by records of paired planktic δ^{18}O and SST running farther apart in Figure 3. Ice rafting in the northwest Pacific ended about 2000 years after the onset of Termination I (~17 cal. ka), and was coeval with a decrease in ^{14}C reservoir ages of pycnocline waters from 1150 to 300 years [*Sarnthein et al.*, 2007]. This drop reflects a relatively rapid transition from stratified to vertically mixed surface waters. It led to ongoing uptake of fresh atmospheric ^{14}C from ~17–11 cal. ka. With some delay the mixing is also reflected by a close match of δ^{18}O and Mg/Ca-based SST records for surface and subsurface waters, in particular after 15 cal. ka (Figure 3). After ~1500 years, mixing finally induced a gradual but major rejuvenation of deepwater ventilation ages from >3600 to <1400 ^{14}C years, which serves as a record of a major oxygenation process that started to culminate after 16.0/14.5 cal. ka (Figure S4a). In addition, short phases of pronounced seasonal sea ice formation led to

production of brinewater plumes and further oxygenation of upper deepwater in the far northwest Pacific during late deglacial times (Figure 3a).

[77] During the early deglacial, vertical mixing was discontinuous, and coeval with three short-term but major SST oscillations from 4° to 10°C at 18–15 cal. ka (Mg/Ca and planktic $\delta^{18}O$ excursions in Figure 3a). Similar warm pulses occurred in the deglacial Kuroshio Current [*Sawada and Handa*, 1998], in contrast to coeval North Atlantic SST which remained at a minimum level over stadial H1 [*Weinelt et al.*, 2003]. This seesaw between North Pacific and North Atlantic SST is characteristic of millennial-scale periods with weak North Pacific surface water stratification according to model experiments of *Schmittner et al.* [2007]. This is precisely the regime identified by our data over large parts of Termination I, unlike today (Figures 3 and 6).

[78] The marked SST highs at MD01-2416 and MD02-2489 (Figures 3a and 3b) may record short-lasting (hundreds to several thousand years long) phases of a far northward expansion of the subtropical North Pacific gyre filled with Kuroshio waters. Vertical mixing in the northwest Pacific then was linked to a distinct culmination of SSS (36 versus 33 psu today), that ended in the early Holocene as soon as SST and SSS started to drop to the present low level near 9 and 6 cal. ka (details by *Sarnthein et al.* [2004]).

5.2. Standard Series of Productivity Events Over Termination I

[79] Over the LGM, planktic $\delta^{13}C$ minima of *N. pachyderma* sin. document high nutrients in subsurface waters of the eastern and western subarctic Pacific. However, strong stratification prevented these nutrients from supporting productivity in surface waters. In the northwest Pacific it occurred only 2000 years after the onset of Termination I, until the end of ice rafting ~17 cal. ka. Subsequent short-lasting pulses of invigorated vertical (winter ?) mixing supplied high nutrients to the euphotic surface waters, and in turn, caused a prominent bloom of algal chlorins (Figure 3a). In contrast, production of diatom biogenic opal in the northwest Pacific reached a similar maximum only a further 1500 years later, 15.8–13.3 cal. ka. Hence, the increased supply of dissolved silica to the subpolar northwest Pacific gyre lagged significantly behind the increase of other nutrients. This was different from Site MD02-2489 in the far northeastern Pacific, where the rise of chlorins and opal was precisely coeval, near ~15 ka, only 4000 years after the onset of Termination I (Figure 3b). This rise matches a striking abrupt SSS decrease by >1 psu (planktic $\delta^{18}O$ decrease in Figure 3b), here ascribed to a meltwater pulse in the Aleutian Current which was a sensitive record of increased freshwater discharge from the Rocky Mountains and enhanced chemical erosion on land [*Weingartner et al.*, 2005].

[80] During this deglacial high-productivity event, concentrations and accumulation rates of chlorins and opal reached a level (e.g., >3–4 g opal cm^{-2} 1000 a^{-1}) that came close to values characteristic of the pre-Quaternary mid-Pliocene at ODP Site 882, when the North Pacific still was subject to large-scale deepwater upwelling [*Haug et al.*, 1999; *Sigman et al.*, 2004] and probably to major silica discharge from North American rivers. Similar productivity peaks were reported for the early last deglacial from the Bering Sea [*Cook et al.*, 2005], various neighboring sites in the northwest Pacific [*Keigwin et al.*, 1992], and off west Canada [*McKay et al.*, 2004], although short-term age control of these records is poorly constrained, since past changes in ^{14}C reservoir ages were largely unknown.

[81] Subsequent to Termination I, the early Holocene peak interglacial was marked by cooling, reduced nutrients in subsurface waters, and low productivity of chlorins and biogenic opal, although vertical mixing started to decrease only gradually, first at northeastern Site MD02-2489 and later in the northwest (Figure 3), as suggested by paired planktic $\delta^{18}O$ records of surface and subsurface waters. Low productivity resulted in less organic fluff at the sea floor in addition to enhanced oxygenation of Pacific Deepwater that persisted since 14.5 cal. ka, as clearly reflected by a distinct coeval increase in epibenthic $\delta^{13}C$ (Figures 3a and 3b, top). The combination of well-ventilated bottom water and reduced organic fluff resulted in an outstanding preservation spike of $CaCO_3$ that represented low productivity during peak interglacial times.

[82] Some proxies don't agree with this deglacial "standard series" of productivity excursions (Figure 6) outlined for Termination I and early MIS 1. Problems concerning $\delta^{15}N_{bulk}$ as a complex proxy of nutrient utilization were already outlined in the Methods section. In addition, the maximum of biogenic Ba at ODP Site 882 (record tuned by means of Ca peaks to the records of MD01-2416 in Figure 5a; *Jaccard et al.* [2005]) does not match the prominent productivity maxima of chlorin and biogenic opal over Termination I. On the contrary, the maxima in Ba_{bio} only occur during the early Holocene, likewise during preceding peak interglacials, when chlorins and biogenic opal already had decreased. Thus the maxima are coeval with pronounced minima in planktic productivity (and in relative nutrient utilization; *Galbraith et al.* [2008]), and on the other hand with prominent preservation spikes of $CaCO_3$, for reasons not properly understood, but in harmony with caveats discussed by *Plewa et al.* [2006]. In contrast to Site 882, a Holocene maximum of biogenic Ba in the Bering Sea (Core JPC 17; *Brunelle et al.* [2007]) slightly precedes that of biogenic opal, but clearly lags behind a deglacial $CaCO_3$ maximum near 15 cal. ka. In the Sea of Okhotsk (Core PC 1, *Sato et al.* [2002]) biogenic Ba likewise increased earlier than opal, however, already during early deglacial times. Obviously the timing of these productivity signals has strongly differed amongst various open Pacific and adjacent sea regions, which implies that results of single records from adjacent sea regions cannot be generalized. Possibly, the Ba maximum was affected by potential early diagenetic remobilization due to changing redox states through time by differential deposition of organic matter (P. Delaney, oral communication, 2008).

[83] Our productivity events in the northwest Pacific agree with the findings of *Crusius et al.* [2004] who suggest that elevated northwest Pacific productivity formed a prime source of low-oxygen, silica-enriched North Pacific Intermediate Water (NPIW) which finally reached the western continental margin of North America. On the basis of

improved age control [*Sarnthein et al.*, 2007] the recirculation of NPIW up to California may have taken approximately 1000 years. In contrast, *Tsunogai* [2002] and *Sarmiento et al.* [2004] surmised that the almost unique wealth of silica in North Pacific near-surface waters and NPIW may originate from direct tapping of upwelled, nutrient-enriched Pacific deepwater. Both these divergent conceptual models, and the search for the final origin of the outstanding high silica concentrations in surface and intermediate waters of the subarctic North Pacific, require extensive future research.

5.3. Productivity Events Over Terminations II–V

[84] On the basis of Core MD01-2416 we may infer that terminations II to V each displayed a largely similar series of changes in ocean circulation as deduced for Termination I and MIS 1 (Figures 4a, 4b, and 5a), although water masses cannot be traced back before 40 cal. ka by means of paleoventilation ages. However, various indirect lines of evidence suggest for each termination an initial period with pulses of strong vertical mixing of surface waters and North Pacific deepwater formation analogous to Termination I, whereas long-term stable surface stratification returned only late, i.e., during peak and late interglacial times (Figure 6).

[85] Accordingly, SST records for each early termination show major millennial-scale oscillations right after the end of IRD supply, except for Termination V. Here short-lasting SST oscillations may be muted by the SIMMAX technique as at Termination I. As in the last deglacial, the early parts of terminations II–V each were marked by high nutrient contents and peaks in algal productivity that may approximately match maxima in relative nutrient utilization and their changing orders of magnitude [*Galbraith et al.*, 2008]. Although the peaks were much lower than during the last deglacial, in contrast to Termination I opal productivity remained generally low, possibly a response to long-term reduced deglacial silica discharge by the Aleutian Current.

[86] As in the standard series of events (Figure 6) peak interglacial stages were marked by maximum SST, already terminating during late interglacial times with a minor (terminations I and IV) or major (terminations III and V) abrupt SST drop (Figures 4a and 4b). Peak MIS 5.5 formed an exception from this rule, with a slight SST increase extending far into the subsequent MIS 5.4, for unknown reasons. As in the early Holocene, all peak interglacial culminations of SST coincided with minima of nutrients and algal productivity, at the same time as paramount maxima of $CaCO_3$ preservation and biogenic Ba (Figure 5a, panel G; *Jaccard et al.* [2005]).

[87] The distinct coolings during late interglacials entailed a renewed, partly abrupt increase in the nutrient concentration of subsurface waters and, because of shallow vertical mixing, a second prominent productivity peak near the end of each interglacial (Figures 5a and 6). Most of these events are recorded by biogenic opal, and a few by chlorins (MIS 5.4 and prior to MIS 7.52). Thus they partly differ from the chlorin-dominated productivity peaks during early terminations. Apparently, the late interglacial productivity events were linked to low SSS (as shown by low planktic $\delta^{18}O$; Figures 4a and 4b) and stratification in the northern North Pacific similar to today, a scenario which may serve as a model for potential productivity regimes of future Holocene millennia. Surface stratification induced by low SSS suggests that the late interglacial productivity peaks resulted less from tapped nutrient sources of Pacific Deepwater than from silica-enriched nutrients from North American rivers. These nutrients spread with the Aleutian Current over the entire subarctic North Pacific, a scenario similar to the late deglacial productivity peak in the far northeastern Pacific (MD02-2489 in Figures 3b and 5b).

5.4. Potential Links to Deglacial Rise in Atmospheric pCO_2

[88] Deglacial maxima of productivity linked to strong vertical mixing and short-term positive SST excursions (Figures 3–6) were coeval with a major deglacial rise in atmospheric pCO_2 by ~45 ppmv 16.7–14.5 cal. ka [*Monnin et al.*, 2001; *Köhler et al.*, 2005]. This rise probably derived from a two-step release of CO_2 from the ocean to the atmosphere, a substantial portion of which may have come from the subarctic North Pacific. In this case our paleoceanographic records imply that increased sequestration of atmospheric carbon during peak productivity was well overcompensated by enhanced degassing of upwelled CO_2 as a result of deep vertical convection. These links likewise applied to glacial terminations I–V. In contrast, the late interglacial productivity maxima that were promoted by major riverine silica supply into a highly stratified North Pacific were probably much less influential on CO_2 exchange between ocean and atmosphere. The biological pump then favored oceanic CO_2 uptake.

6. Conclusions

[89] Meridional overturning circulation in the northern North Pacific may play a major role for changes in the CO_2 budget of the global ocean. However, pertinent long and high-resolution paleoceanographic records from this region are rare. IMAGES long cores MD01-2416 and MD02-2489 from the subarctic northwest and northeast Pacific now provide the first multiproxy records of past changes in vertical mixing of water masses, nutrient concentrations, and algal productivity with centennial-to-millennial-scale resolution, focusing on the last five glacial terminations and subsequent interglacials. Tracers of SST, surface water stratification, detailed age control, and ^{14}C paleoreservoir ages of surface and deep waters served to unravel short-term ocean processes that may have controlled past changes in productivity over the last 450 ka.

[90] The high sedimentation rates of Termination I and MIS 1 enabled us to extract a standard sequence of short-lasting highs and lows in productivity and the admixture of nutrients for deglacial and interglacial times (Figure 6). This sequence largely applies also to productivity changes of terminations II to V, although most of them were less pronounced. High nutrients in subsurface waters were characteristic of early terminations and antecedent glacials. Ice rafting only terminated up to 2000 years after the end of peak glacial times and implied an immediate start of vertical mixing of surface waters and thus, a first productivity bloom as documented by peaks of chlorins. During Termination I, a

maximum of biogenic opal production followed some 1000 years later. During late deglacial to early interglacial times, nutrients and productivity had ceased to a minimum, whereas deepwater continued to be ventilated, which led to a paramount maximum of $CaCO_3$ preservation in the deep sea (Figures 3, 5a, and 5b). Concentration maxima of biogenic Ba [*Jaccard et al.*, 2005] precisely coincide with these minima in chlorin and opal production after terminations I to V. Accordingly, the origin of Ba peaks as potential productivity proxies is considered problematic. Interglacials ended with a second productivity peak of biogenic opal, and frequently of chlorins (Figures 5a and 5b), when stable stratification of surface waters was reinstalled by increased freshwater input lowering SSS.

[91] The origin of this sequence of productivity events can be largely constrained at Termination I on the basis of short-term variations in surface and deepwater reservoir ages and paired planktic $\delta^{18}O$ and SST records of vertical mixing of surface waters. The records show a peak glacial period of stable surface stratification lasting until ~17 ka, subsequently an interval of strongly fluctuating but vivid vertical mixing and SST oscillations, and also high deepwater ventilation that continued until <10 ka. Stable surface water stratification was reinstalled near the end of the early and middle Holocene (~9 ka, 6 ka), coeval with major drops in SST and SSS. An analogous suite of changes probably controlled the preceding terminations II to V and associated peak interglacials, except for a long-term continuation of high SST at the end of MIS 5.5 far into MIS 5.4, as yet unexplained.

[92] High chlorin productivity appears closely tied to macronutrient supply from subsurface waters during times of vertical mixing. By contrast, maxima in opal productivity may have either been controlled by nutrients derived from upwelled Pacific Deepwater and/or by extensive silica supply through rivers from western North America. In harmony with this model, the productivity maximum of opal in northeast Pacific Core MD02-2489 near 15 cal. ka was tied to an abrupt reduction of SSS by >1 psu in the Aleutian Current, probably strongly influenced by North American river and meltwater discharge.

[93] Early deglacial vertical mixing and maxima in chlorin productivity matched a short-term major rise in atmospheric CO_2. Enhanced release of oceanic CO_2 from the North Pacific may then have played a major role in the global carbon budget. In contrast, maxima in opal production concurred with low SSS, stable surface stratification, and minor release of oceanic CO_2, in particular near the end of past interglacial stages. Accordingly, culminating opal production and significant CO_2 drawdown by the North Pacific biological pump may serve as a viable scenario for the future end of the Holocene.

[94] **Acknowledgments.** We are grateful to Eric Galbraith for extensive spirited and stimulating discussions. Initially divergent interpretations between our twin manuscripts (*Galbraith et al.* [2008] and this paper) were reduced to a minimum through extensive correspondence. Remaining divergencies in interpretation of available data are defined in the text for outside readers. Inspiring help came from two careful reviews of our manuscript and Gerald Dickens as journal editor. Neville Exon (Canberra) greatly helped us with editing the final text version. We thank Mara Weinelt and Uwe Pflaumann (Kiel) and Michal Kucera (Tübingen) for valuable scientific advice and discussions, Claudia Sieler (Kiel) for data management. Dörte Gudehus and Karin Kissling helped with picking foraminifera samples for stable isotope analyses, in the beginning supervised by C. Bühring. All of them and Jutta Heinze provided efficient and careful laboratory assistance. We thank H. Erlenkeuser and his team at the Leibniz Laboratory of Kiel University for measuring with care large numbers of stable isotope data on partly very low foraminiferal specimen numbers. We acknowledge the Leibniz Laboratory for precise and fast measurements of AMS radiocarbon ages. Liane Brück provided valuable technical assistance with paleomagnetic analyses, Thomas Frederichs, Christian Hilgenfeldt, and Karl Fabian (Bremen) software to analyze paleomagnetic data. We thank the crew on board of RV Marion Dufresne, in particular Yvon Balut, for retrieving the 45- and 30-m-long piston cores MD01-2416 and MD02-2489. Generous funding for core retrieval and scientific evaluation of core samples came from the Deutsche Forschungsgemeinschaft (DFG) (grants Sa 207/43-1 and 2).

References

Asahi, H., and K. Takahashi (2007), A 9-year time-series of planktonic foraminifer fluxes and environmental change in the Bering Sea and the central subarctic Pacific Ocean, 1990–1999, *Progr. Oceanogr.*, *72*, 343–363.

Barker, S., M. Greaves, and H. Elderfield (2003), A study of cleaning procedures used for foraminiferal Mg/Ca paleothermometry, *Geochem. Geophys. Geosyst.*, *4*(9), 8407, doi:10.1029/2003GC000559.

Bassinot, F. C., L. D. Labeyrie, E. Vincent, X. Quidelleur, N. J. Shackleton, and Y. Lancelot (1994), The astronomical theory of climate and the age of the Brunhes-Matuyama magnetic reversal, *Earth Planet. Sci. Lett.*, *126*, 91–108.

Bassinot, F. C., C. Waelbroeck, and Shipboard Scientific Party (2002), IMAGES VII Cruise Report, *Les Publications de l'Institut Français pour la Recherche et la Technologie Polaires. Les rapports de campagnes à la mer*, *01*, 435 pp., l'Inst. Français pour la Rech. et la Technol. Polaires, Plouzane, France.

Bauch, D., and H. A. Bauch (2001), Last glacial benthic foraminiferal $\delta^{18}O$ anomalies in the polar North Atlantic: A modern analogue evaluation, *J. Geophys. Res.*, *106*, 9135–9143.

Broecker, W. S. (1991), The great ocean conveyor, *Oceanography*, *4*, 79–89.

Brunelle, B. G., D. M. Sigman, M. S. Cook, L. D. Keigwin, G. H. Haug, B. Plessen, G. Schettler, and S. L. Jaccard (2007), Evidence from diatom-bound nitrogen isotopes for subarctic Pacific stratification during last ice age and a link to North Pacific denitrification changes, *Paleoceanography*, *22*, PA1215, doi:10.1029/2005PA001205.

Calvert, S. E., J. S. Vogel, and J. R. Southon (1987), Carbon accumulation rates and the origin of the Holocene sapropel in the Black Sea, *Geology*, *15*, 918–921.

Chen, M.-T., C.-C. Huang, U. Pflaumann, C. Waelboeck, and M. Kucera (2005), Estimating glacial western Pacific sea-surface temperature: Methodological overview and data compilation of surface sediment planktic foraminifer faunas, *Quat. Sci. Rev.*, *24*, 1049–1062.

Clarke, A., J. Church, and J. Gould (2001), Ocean processes and climate phenomena, in *Ocean Circulation and Climate*, *Int. Geophys. Ser.*, vol. 77, edited by G. Siedler, J. Church, and J. Gould, pp. 11–30, Acad. Press, San Diego, Calif.

CLIMAP Project Members (CLIMAP) (1981), Seasonal reconstructions of the Earth's surface at the Last Glacial Maximum, *Map Chart Ser. MC-36*, Geol. Soc. Am., Boulder, Colo.

Cook, M. S., L. D. Keigwin, and C. A. Sancetta (2005), The deglacial history of surface and intermediate water of the Bering Sea, *Deep Sea Res., Part II*, *52*, 2163–2173.

Crusius, J., T. F. Pedersen, S. Kienast, L. Keigwin, and L. Labeyrie (2004), Influence of northwest Pacific productivity on North Pacific Intermediate Water oxygen concentrations during the Bølling-Ållerød interval (14.7–12.9 ka), *Geology*, *32*, 633–636.

Darling, K. F., M. Kucera, C. M. Wade, P. von Langen, and D. Pak (2003), Seasonal distribution of genetic types of planktonic morphospecies in the Santa Barbara Channel and its paleoceanographic implications, *Paleoceanography*, *18*(2), 1032, doi:10.1029/2001PA000723.

Darling, K., M. Kucera, and C. Wade (2006), Quaternary climate instability as the driver of genetic diversification in *Neogloboquadrina pachyderma* (sin), *Anuário do Inst. de Geociências-UFRJ*, *29*, 533.

De La Rocha, C. L. (2007), The biological pump, in *Treatise on Geochemistry*, vol. 6, 2nd ed., edited by H. Elderfield, pp. 83–111, Elsevier, Amsterdam.

DeMaster, D. J. (1981), The supply and accumulation of silica in the marine environment, *Geochim. Cosmochim. Acta*, *45*, 1715–1732.

Deuser, W. G., E. H. Ross, C. Hemleben, and M. Spindler (1981a), Seasonal changes in species composition numbers, mass, size and isotopic composition of planktonic foraminifera settling into the deep Sargasso Sea, *Palaeogeogr. Palaeoclimatol. Palaeoecol.*, *33*, 103–127.

Deuser, W. G., E. H. Ross, and R. F. Anderson (1981b), Seasonality in the supply of sediment to the deep Sargasso Sea and implications for the rapid transfer of matter to the deep ocean, *Deep Sea Res., Part A*, *28*, 495–505.

de Villiers, S., M. Greaves, and H. Elderfield (2002), An intensity ratio calibration method for the accurate determination of Mg/Ca and Sr/Ca of marine carbonates by ICP-AES, *Geochem. Geophys. Geosyst.*, *3*(1), 1001, doi:10.1029/2001GC000169.

Dodimead, A. J., F. Favorite, and T. Hirano (1963), Salmon of the North Pacific Ocean, Part II: Review of oceanography of the Subarctic Pacific Ocean, *Int. North Pacific Fisheries Comm. Bull.*, *13*, 1–195.

Duplessy, J.-C., N. J. Shackleton, R. G. Fairbanks, L. D. Labeyrie, D. Oppo, and N. Kallel (1988), Deepwater source variations during the last climatic cycle and their impact on the global deepwater circulation, *Paleoceanography*, *3*, 343–360.

Duplessy, J. C., L. Labeyrie, A. Juillet-Leclerc, F. Maitre, J. Duprat, and M. Sarnthein (1991a), Surface salinity reconstruction of the North Atlantic Ocean during the Last Glacial Maximum, *Ocean. Acta*, *14*, 311–324.

Duplessy, J.-C., E. Bard, M. Arnold, N. J. Shackleton, J. Duprat, and L. D. Labeyrie (1991b), How fast did the ocean-atmosphere system run during the last deglaciation?, *Earth Planet. Sci. Lett.*, *103*, 27–40.

Ebbesmeyer, C. C., W. J. Ingraham, T. C. Royer, and C. E. Grosch (2007), Tub toys orbit the Pacific Subarctic Gyre, *Eos Trans. AGU*, *88*(1), doi:10.1029/2007EO010001.

Elderfield, H., and G. Ganssen (2000), Past temperature and d18O of ocean surface waters inferred from foraminiferal Mg/Ca ratios, *Nature*, *405*, 442–445.

EPICA community members, (2004), Eight glacial cycles from an Antarctic ice core, *Nature*, *429*, 623–628.

Galbraith, E. D., M. Kienast, S. J. Jaccard, T. F. Pedersen, B. G. Brunelle, D. M. Sigman, and T. Kiefer (2008), Consistent relationship between global climate and surface nitrate utilization in western Subarctic Pacific throughout last 500 ka, *Paleoceanography*, *23*, PA2212, doi:10.1029/2007PA001518.

Ganssen, G. (1983), Dokumentation von küstennahem Auftrieb anhand stabiler Isotope in rezenten Foraminiferen vor Nordwest-Afrika, *Meteor Forsch. Erg.*, *C37*, 1–46.

Gordon, A. L. (1991), The role of thermohaline circulation in global climate change, *Lamont-Doherty Earth Obs. Rep.*, *1990–1991*, 44–51.

Guyodo, Y., and J. P. Valet (1999), Global changes in intensity of the Earth's magnetic field during the past 800 kyr, *Nature*, *399*, 249–252.

Haug, G. H., D. M. Sigman, R. Tiedemann, T. F. Pedersen, and M. Sarnthein (1999), Onset of permanent stratification in the subarctic Pacific Ocean, *Nature*, *401*, 779–782.

Hedges, J. I., and R. G. Keil (1995), Sedimentary organic matter preservation: an assessment and speculative synthesis, *Mar. Chem.*, *49*, 81–115.

Jaccard, S. L., G. H. Haug, D. M. Sigman, T. F. Pedersen, H. R. Thierstein, and U. Röhl (2005), Glacial/interglacial changes in subarctic North Pacific stratification, *Science*, *308*, 1003–1006.

Keigwin, L. D. (1998), Glacial-age hydrography of the far northwest Pacific Ocean, *Paleoceanography*, *13*, 323–339.

Keigwin, L. D., G. A. Jones, and P. N. Froelich (1992), A 15,000 year paleoenvironmental record from Meiji Seamount, far northwestern Pacific, *Earth Planet. Sci. Lett.*, *111*, 425–440.

Kirschvink, J. L. (1980), The least-squares line and plane and the analysis of paleomagnetic data, *Geophys. J. Res. Astr. Soc.*, *62*, 699–718.

Köhler, P., H. Fischer, G. Munhoven, and R. E. Zeebe (2005), Quantitative interpretation of atmospheric carbon records over the last glacial termination, *Global Biogeochem. Cycles*, *19*, GB4020, doi:10.1029/2004GB002345.

Kucera, M., and K. F. Darling (2002), Genetic diversity among modern planktonic foraminifer species: its effects on paleoceanographic reconstructions, *Philos. Trans. R. Soc. London Ser. A*, *360*, 695–718.

Labeyrie, L., and J.-C. Duplessy (1985), Changes in the oceanic $^{13}C/^{12}C$ ratio during the last 140,000 years: High latitude surface water records, *Palaeogeogr. Palaeoclimatol. Palaeoecol.*, *50*, 217–240.

Labeyrie, L. D., J.-C. Duplessy, and P. L. Blanc (1987), Variations in mode of formation and temperature of oceanic deep waters over the past 125,000 years, *Nature*, *327*, 477–482.

Lynch-Stieglitz, J. (2003), Tracers of past ocean circulation, in *Treatise on Geochemistry, 6*, edited by H. Elderfield, pp. 433–451, Elsevier, Amsterdam.

Mackensen, A., H.-W. Hubberten, T. Bickert, G. Fischer, and D. K. Fütterer (1993), The ^{13}C in benthic foraminiferal tests of *Fontbotia wuellerstofi* (Schwager) relative to ^{13}C of dissolved inorganic carbon in southern ocean deep water: Implications for glacial ocean circulation models, *Paleoceanography*, *8*, 587–610.

McKay, J. L., T. F. Pedersen, and S. S. Kienast (2004), Organic carbon accumulation over the last 16 kyr off Vancouver Island, Canada: Evidence for increased marine productivity during the deglacial, *Quat. Sci. Rev.*, *23*, 261–281.

Monnin, E., A. Indermühle, A. Dällenbach, J. Flückiger, B. Stauffer, T. F. Stocker, D. Raynaud, and J.-M. Barnola (2001), Atmospheric CO_2 concentrations over the last glacial termination, *Science*, *291*, 112–114.

Müller, P. J., and R. Schneider (1993), An automated leaching method for the determination of opal in sediments and particulate matter, *Deep Sea Res., Part I*, *40*, 425–444.

Müller, P. J., and E. Suess (1979), Productivity, sedimentation rate and sedimentary organic matter in the oceans: 1. Organic carbon preservation, *Deep Sea Res., Part A*, *26*, 1347–1362.

Paillard, D., L. Labeyrie, and P. Yiou (1996), Macintosh program performs time-series analyses, *Eos Trans. AGU*, *71*, 379.

Pflaumann, U., et al. (2003), Glacial North Atlantic: Sea-surface conditions reconstructed by GLAMAP 2000, *Paleoceanography*, *18*(3), 1065, doi:10.1029/2002PA000774.

Plewa, K., H. Meggers, and S. Kasten (2006), Barium in sediments off northwest Africa: A tracer for paleoproductivity or meltwater events?, *Paleoceanography*, *21*, PA2015, doi:10.1029/2005PA001136.

Reimer, P. J., et al. (2004), INTCAL04 terrestrial radiocarbon age calibration, 0–26 cal kyr BP, *Radiocarbon*, *46*, 1029–1058.

Roden, G. I. (1995), Aleutian Basin of the Bering Sea: Thermohaline, oxygen, nutrient, and current structure in July 1993, *J. Geophys. Res.*, *100*, 13,539–13,554.

Röhl, U., and L. J. Abrams (2000), High-resolution, downhole and non-destructive core measurements from sites 999 and 1001 in the Caribbean Sea: Application to the late Paleocene Thermal Maximum, *Proc. Ocean Drill. Progr., Sci. Res.*, *165*, 191–203.

Sarmiento, J. L., N. Gruber, M. A. Brzezinski, and J. P. Dunne (2004), High-latitude controls of thermocline nutrients and low latitude biological productivity, *Nature*, *427*, 56–60.

Sarnthein, M., U. Pflaumann, R. Ross, R. Tiedemann, and K. Winn (1992), Transfer functions to reconstruct ocean paleoproductivity, a comparison, in *Evolution of Upwelling Systems since the Early Miocene*, *Geol. Soc. Spec. Publ.*, vol. 63, edited by C. Summerhayes et al., pp. 411–437, London.

Sarnthein, M., K. Winn, S. J. A. Jung, J.-C. Duplessy, L. Labeyrie, H. Erlenkeuser, and G. Ganssen (1994), Changes in East Atlantic deep water circulation over the last 30,000 years: Eight time slice reconstructions, *Paleoceanography*, *9*, 209–268.

Sarnthein, M., et al. (1995), Variations in Atlantic surface ocean paleoceanography, 50°–85°N: A time-slice record of the last 30,000 years, *Paleoceanography*, *10*, 1063–1094.

Sarnthein, M., et al. (2001), Fundamental modes and abrupt changes in North Atlantic circulation and climate over the last 60 ky: Concepts, reconstruction and numerical modelling, in *The Northern Atlantic: A Changing Environment*, edited by P. Schäfer et al., pp. 365–410, Springer, Berlin.

Sarnthein, M., H. Gebhardt, T. Kiefer, M. Kucera, M. Cook, and H. Erlenkeuser (2004), Mid Holocene origin of the sea surface salinity low in the subarctic North Pacific, *Quat. Sci. Rev.*, *23*, 2089–2099.

Sarnthein, M., H. Gebhardt, T. Kiefer, H. Erlenkeuser, C. Kissel, and F. Schmieder (2005), 95-Ky Cycles of ocean circulation in the far northwestern Pacific and South China Sea during the Brunhes Chron, in *Milutin Milankovitch Anniversary Symposium: Paleoclimate and the Earth Climate System, Serbian Academy of Sciences and Arts*, vol. 110, edited by A. Berger, M. Ercegovac, and F. Mesinger, pp. 135–140, Serbian Acad. of Sci. and Arts, Belgrade.

Sarnthein, M., T. Kiefer, P. M. Grootes, and H. Elderfield (2006), Warmings in the far northwestern Pacific promoted pre-Clovis immigration to America during Heinrich Event 1, *Geology*, *34*, 141–144.

Sarnthein, M., P. M. Grootes, J. P. Kennett, and M.-J. Nadeau (2007), ^{14}C Reservoir ages show deglacial changes in ocean currents and carbon cycle, in *Past and Future Changes of the Oceanic Meridional Overturning Circulation: Mechanisms and Impacts*, *AGU Monogr. Ser.*, vol. 173, 175–196.

Sato, M. M., H. Narita, and S. Tsunogai (2002), Barium increasing prior to opal during the last termination of glacial ages in the Okhotsk Sea sediments, *J. Oceanogr.*, *58*, 461–467.

Sawada, K., and N. Handa (1998), Variability of the path of the Kuroshio ocean current over the past 25,000 years, *Nature*, *392*, 592–595.

Schlosser, P., J. L. Bullister, R. A. Fine, W. J. Jenkins, R. Key, J. Lupton, W. Roether, and W. M. J. Smethie (2001), Transformation of age and water masses, in *Ocean Circulation and Climate*, *Int. Geophys. Ser.*, vol. 77, edited by G. Siedler, J. Church, and J. Gould, pp. 431–452, Acad. Press, San Diego, Calif.

Schmittner, A., E. D. Galbraith, S. W. Hostetler, T. F. Pedersen, and R. Zhang (2007), Large fluctuations of dissolved oxygen during Dansgaard-Oeschger oscillations caused by variations of North Atlantic Deep Water subduction, *Paleoceanography*, *22*, PA3207, doi:10.1029/2006PA001384.

Schmitz, W. J. (1995), On the interbasin-scale thermohaline circulation, *Rev. Geophys.*, *33*, 151–173.

Sigman, D. M., and E. A. Boyle (2000), Glacial/interglacial variations in atmospheric carbon dioxide, *Nature*, *407*, 859–869.

Sigman, D. M., S. L. Jaccard, and G. H. Haug (2004), Polar ocean stratification in a cold climate, *Nature*, *428*, 59–63.

Simstich, J. (1998), Die ozeanische Deckschicht des Europäischen Nordmeers im Abbild stabiler Isotope von Kalkgehäusen unterschiedlicher Planktonforaminiferenarten, D.Sc. thesis, 83 pp., Univ. of Kiel, Germany.

Simstich, J., M. Sarnthein, and H. Erlenkeuser (2002), Paired δ^{18}O signals of *N. pachyderma* (s) and *T. quinqueloba* show thermal stratification structure in the Nordic Seas, *Mar. Micropaleontol.*, *48*, 107–125.

Singer, B. S., M. K. Relle, K. A. Hoffmann, A. Battle, C. Laj, H. Guillou, and J. C. Carracedo (2002), Ar/Ar ages from transitionally magnetized lavas on La Palma, Canary Islands, and the geomagnetic instability timescale, *J. Geophys. Res.*, *107*(B11), 2307, doi:10.1029/2001JB001613.

Singer, B. S., K. A. Hoffmann, R. S. Coe, L. L. Brown, B. R. Jicha, M. S. Pringle, and A. Chauvin (2005), Structural and temporal requirements for geomagnetic field reversals deduced from lava flows, *Nature*, *434*, 633–636.

Southon, J. R., and D. Fedje (2003), A post-glacial record of ^{14}C reservoir ages for the British Columbia coast, *Can. J. Archeol.*, *27*, 95–111.

Southon, J. R., S. Gorbarenko, M. Kashgarian, D. Fedje, R. McNeely, A. Dyke, and B. Lynn (2005), Reservoir ages within the North Pacific Subarctic Gyre, paper presented at 10th International Conference on Accelerator Mass Spectrometry, University of California, Berkeley, Calif., 5–10 September.

Széréméta, N., F. Bassinot, Y. Balut, L. Labeyrie, and M. Pagel (2004), Oversampling of sedimentary series collected by giant piston corer: evidence and corrections based on 3.5-kHz chirp profiles, *Paleoceanography*, *19*, PA1005, doi:10.1029/2002PA000795.

Takahashi, T., et al. (2002), Global sea-air CO_2 flux based on climatological surface ocean pCO2, and seasonal biological and temperature effects, *Deep Sea Res., Part II*, *49*, 1601–1622.

Thouveny, N., J. Carcaillet, E. Moreno, G. Leduc, and D. Nérini (2004), Geomagnetic moment variation and paleomagnetic excursions since 400 kyr BP: A stacked record from sedimentary sequences of the Portuguese margin, *Earth Planet. Sci. Lett.*, *219*, 377–396.

Tjallingii, R., U. Röhl, M. Kölling, and T. Bickert (2007), Influence of the water content on X-ray fluorescence core scanning measurements in soft marine sediments, *Geochem. Geophys. Geosyst.*, *8*, Q02004, doi:10.1029/2006GC001393.

Tsuda, A., et al. (2003), A mesoscale iron enrichment in the western subarctic Pacific induces a large centric diatom bloom, *Science*, *300*, 958–961.

Tsunogai, S. (2002), The western North Pacific playing a key role in global biogeochemical fluxes, *J. Oceanogr.*, *58*, 245–257.

Wang, L., M. Sarnthein, H. Erlenkeuser, J. Grimalt, P. Grootes, S. Heilig, E. Ivanova, M. Kienast, C. Pelejero, and U. Pflaumann (1999), East Asian monsoon climate during the late Pleistocene: High-resolution sediment records from the South China Sea, *Mar. Geol.*, *156*, 245–284.

Warren, B. (1983), Why is no deep water formed in the North Pacific?, *J. Mar. Res.*, *41*, 327–347.

Weinelt, M., E. Vogelsang, M. Kucera, U. Pflaumann, M. Sarnthein, A. Voelker, H. Erlenkeuser, and B. A. Malmgren (2003), Variability of North Atlantic heat transfer during MIS 2, *Paleoceanography*, *18*(3), 1071, doi:10.1029/2002PA000772.

Weingartner, T. J., S. L. Danielson, and T. C. Royer (2005), Freshwater variability and predictability in the Alaskan Coastal Current, *Deep Sea Res., Part II*, *52*, 161–191.

Yool, A., and T. Tyrrell (2003), Role of diatoms in regulating the ocean's silicon cycle, *Global Biogeochem. Cycles*, *17*(4), 1103, doi:10.1029/2002GB002018.

Zahn, R., T. F. Pedersen, B. D. Bornhold, and A. C. Mix (1991), Water mass conversion in the glacial subarctic Pacific (54°N, 148°W): Physical constrains and the benthic-planktonic stable isotope record, *Paleoceanography*, *6*, 543–560.

H. Gebhardt, Geologische Bundesanstalt, Neulinggasse 38, A-1030 Wien, Austria. (holger.gebhardt@geologie.ac.at)

P. M. Grootes, Leibniz Laboratory, University of Kiel, Olshausenstrasse 40, D-24118 Kiel, Germany.

T. Kiefer, PAGES International Project Office, Sulgeneckstrasse 38, CH-3007 Bern, Switzerland.

H. Kuehn and M. Sarnthein, Institut für Geowissenschaften, University of Kiel, Olshausenstr. 40, D-24118 Kiel, Germany.

U. Röhl and F. Schmieder, Center for Marine Environmental Sciences, University of Bremen, Leobener Strasse, D-28359 Bremen, Germany.